ELSEVIER

J. Non-Newtonian Fluid Mech. 114 (2003) 109–148

Journal of Non-Newtonian Fluid Mechanics

www.elsevier.com/locate/jnnfm

Turbulent pipe flow predictions with a low Reynolds number k–ε model for drag reducing fluids

D.O.A. Cruz [a], F.T. Pinho [b,*]

[a] *Departamento de Engenharia Mecânica, Universidade Federal do Pará-UFPa, Campus Universitário do Guamá, 66075-900 Belém, Pará, Brazil*

[b] *Centro de Estudos de Fenómenos de Transporte, DEMEGI, Faculdade de Engenharia, Universidade do Porto, Rua Dr. Roberto Frias, 4200-465 Oporto Portugal*

Received 20 January 2003; received in revised form 23 June 2003

Abstract

A low Reynolds number k–ε turbulence model is developed for predicting turbulent wall flows of viscoelastic fluids. The model uses a non-linear molecular viscosity that is affected by the turbulent fluctuations and a new damping function is introduced to account for near-wall effects. This new function was made equal to the eddy viscosity damping function which was derived taking into account viscometric and elastic effects.

Flow predictions compare favourably with results from experiments with several viscoelastic fluids, especially the friction factor and the mean velocity. Comparisons of the turbulence kinetic energy are less good, but the model is able to capture the shift of the peak turbulence kinetic energy and rate of dissipation away from the wall, the decrease in those peak values and of the production of k, and the Reynolds shear stress deficit across the pipe. An advantage of the present single-point turbulence closure relative to previous attempts at modelling polymer drag reduction, is the fact that here the input is only the mean velocity and fluid properties and no other modifications of the turbulence model are required to deal with different fluids.

Further developments of the turbulence model are suggested at the end.

1. Introduction

The development of turbulence models for engineering applications in duct flows of drag reducing fluids has not received the attention it deserves. Most of the effort took place in the late 1970s [1–5], some attempts were also made in the 1980s [6], but the outcome was rather limited. Those turbulence models usually consisted of the Newtonian formulation with ad hoc modifications to the numerical values of their

* Corresponding author. Tel.: +351-225-081-762; fax: +351-225-081-763.
E-mail addresses: doac@ufpa.br (D.O.A. Cruz), fpinho@fe.up.pt (F.T. Pinho).

0377-0257/$ – see front matter © 2003 Elsevier B.V. All rights reserved.
doi:10.1016/S0377-0257(03)00119-8

Nomenclature

A	Van Driest's parameter
A_ε	turbulence model parameter
B	parameter defined in Eq. (7)
C	turbulence model parameter in $f_{\mu\mathrm{e}}$
C_{ε_1}	turbulence model parameter
C_{ε_2}	turbulence model parameter
C_{ε_4}	new turbulence model parameter
C_μ	turbulence model parameter
DR	drag reduction intensity, Eq. (51)
f	Darcy's friction factor
f_F	Fanning friction factor
f_μ	damping function of eddy viscosity
f_ν	damping function of molecular viscosity
$f_{\mu\mathrm{e}}$	extensional contribution to eddy viscosity damping function
$f_{\mu\mathrm{v}}$	viscometric contribution to eddy viscosity damping function
$f(y)$	expression quantifying the decay of fluid oscillations in Stokes' second problem
f_1	damping function in ε equation
f_2	damping function in ε equation
k	turbulent kinetic energy
K_e	viscosity consistency index of Trouton ratio behaviour
K_v	viscosity consistency index of shear behaviour
m	parameter defined in Eq. (6)
n	viscosity power index of shear behaviour
p	viscosity power index of Trouton ratio behaviour
$\bar{p}$	mean pressure
P_k	turbulence production, defined in Eq. (15)
r	radial coordinate
R_T	turbulent Reynolds number, defined in Eq. (22)
Re_ap	Reynolds number based on apparent viscosity
Re_w	wall Reynolds number
S	rate of deformation tensor
t	time
u	local mean velocity
u_τ	friction velocity
U	axial mean velocity
U_0	amplitude of oscillating wall in Stokes' second problem
x	axial coordinate
y	distance measured from the wall
y^+	wall coordinate, defined in Eq. (21)
y^+_DM	wall coordinate, defined in Eq. (37)
y^+_w	wall coordinate, defined in Eq. (23)

Greek symbols

$\dot{\gamma}$	invariant measurement of the shear rate
ε	rate of dissipation of turbulent kinetic energy
$\dot{\varepsilon}$	invariant measurement of the strain rate
$\tilde{\varepsilon}$	modified rate of dissipation of turbulent kinetic energy
η_{e}	extensional or elongational viscosity
η_{v}	shear (viscometric) viscosity
μ	molecular viscosity
$\bar{\mu}$	true average molecular viscosity
$\bar{\mu}_{\mathrm{h}}$	time-average molecular viscosity due to high Reynolds number turbulence
ν_{T}	eddy viscosity
ρ	fluid density
$-\rho\overline{uv}$	Reynolds shear stress
σ	stress tensor
σ_k	turbulent Prandtl number for k
σ_ε	turbulent Prandtl number for ε
ω	frequency of oscillating wall in Stokes' second problem

Subscript

w	based on wall conditions

Superscript

$+$	designates quantities normalised with wall coordinates

parameters which depended on the fluid and flow to be predicted and did not take full account of fluid rheology.

The focus of research has been on gaining more understanding of the problem either experimentally, as by Warholic et al. [7,8] and Escudier et al. [9], or numerically by performing various types of DNS investigations which were reviewed in the first part of this work [10]. The time is now right to attempt to develop a turbulence model coupled with viscoelastic fluid rheology, as shown in the introduction of Pinho [10], and following on his steps.

Adopting a modified version of a generalised Newtonian fluid (GNF), Pinho [10] derived the transport equations of momentum, Reynolds stress, turbulent kinetic energy and its rate of dissipation and then performed an order of magnitude analysis to identify the relevant terms and those that could safely be neglected. The paper then concentrated on developing a closure for a k–ε model, but no details were given of the specific values and forms of the parameters and damping functions, and no predictions were carried out, or comparisons made, with experimental data.

This work completes the development of the turbulence model: it provides those missing details, performs simulations of pipe flow with viscoelastic polymer solutions, comparing the corresponding results with experimental data, and assesses the effects of some fluid properties on the capabilities of the turbulence model.

The paper is organised as follows. In Section 2 the equations to be solved and the turbulence model are presented. Section 3 completes the model description by providing numerical values of the parameters and deriving the damping functions for the eddy (f_μ) and molecular viscosities (f_ν). The results of the simulations are presented and discussed in Section 4 and the paper ends with the main conclusions and a summary of future developments.

2. Rheological and transport equations

2.1. The fluid constitutive model

As a constitutive model the GNF of Eq. (1) is adopted, where the variable viscosity function μ is given by Eq. (2):

$$\sigma = 2\mu\mathbf{S}, \tag{1}$$

$$\mu = K_\mathrm{v}[\dot\gamma^2]^{(n-1)/2} K_\mathrm{e}[\dot\varepsilon^2]^{(p-1)/2}. \tag{2}$$

The viscosity combines shear-thinning and strain-thickening dependence, the latter in an attempt to mimic the effect of extensional viscosity on turbulent flow, as explained in [10]. The viscometric behaviour of the fluid is expressed by the first part of Eq. (2)

$$\eta_\mathrm{v} = K_\mathrm{v}[\dot\gamma^2]^{(n-1)/2}, \tag{3}$$

where the consistency and power law indices K_v and n are obtained by least-square fitting to viscometric viscosity data. To introduce the strain-rate dependence into the viscosity model (μ), while respecting some physical constraints and homogeneity, expression (3) is multiplied by the following ratio of the extensional (η_e) to the viscometric (η_v) viscosities:

$$\frac{1}{3}\frac{\eta_\mathrm{e}(\dot\varepsilon)}{\eta_\mathrm{v}(\dot\gamma)} = K_\mathrm{e}[\dot\varepsilon^2]^{(p-1)/2}, \tag{4}$$

leading to the final form of Eq. (2). Note that $\dot\gamma$ and $\dot\varepsilon$ are measurements of the shear and strain rates calculated from invariants of the rate of deformation tensor (see Eqs. (4) and (5) in [10]).

The 1/3 coefficient is necessary to guarantee that, for purely viscous fluids, the viscometric behaviour is fully recovered as it is known from continuum mechanics that inelastic fluids have a Trouton ratio of 3.[1] The above ratio must be calculated at $\dot\gamma = \sqrt{3}\dot\varepsilon$ for reasons explained in [11].

We recommend that the experimental data for the extensional viscosity be fitted by a power law type of equation, and then divided by $3K_\mathrm{v}|\sqrt{3}\dot\varepsilon|^{n-1}$, in this way providing both the coefficient K_e and index p.

Since the viscosity is a non-linear function of fluctuating kinematic tensors, it also fluctuates and this leads to the definition of average and fluctuating viscosities. An expression for the time-average molecular viscosity at high Reynolds number turbulence was derived in detail by Pinho [10], which is in closed form once k and ε are known, and is given by

$$\bar\mu_\mathrm{h} = (C_\mu\rho)^{3m(m-1)A_2/(8+3m(m-1)A_2)} 2^{4m(m-1)A_2/(8+3m(m-1)A_2)} k^{6m(m-1)A_2/(8+3m(m-1)A_2)} \times \varepsilon^{[8-3(m-1)A_2]m/(8+3m(m-1)A_2)} B^{8/(8+3m(m-1)A_2)}, \tag{5}$$

[1] Trouton ratio $T_\mathrm{R} \equiv \eta_\mathrm{e}(\dot\varepsilon)/\eta_\mathrm{v}(\dot\gamma)$.

where $A_2 = 0.45$ [10], and m and B are given by Eqs. (6) and (7), respectively. k and ε stand for the turbulence kinetic energy $k \equiv \bar{u}_{ii}^2/2$ and its rate of dissipation, respectively:

$$m \equiv \frac{n+p-2}{n+p}, \tag{6}$$

$$B = \left[\frac{K_\mathrm{v} K_\mathrm{e}}{A_\varepsilon^{p-1}}\right]^{1-m} 2^{[(n-1)-m(n+1)]/2} \rho^m. \tag{7}$$

A_ε must be higher than $\sqrt{3/2}$ and quantifies the ratio between the fluctuating strain and shear rates [10]. From a parametric investigation onto its effects upon the model predictions a numerical value of 10 was chosen. The coefficient C_μ is standard in k–ε models and its value is discussed in the next section.

The effect of turbulence on the average viscosity $\bar{\mu}_\mathrm{h}$, via the non-linear dependence on $\dot{\gamma}$ and $\dot{\varepsilon}$, appears through the two terms of Eq. (5) containing k and ε. In the absence of shear-rate and strain-rate dependence, a constant viscosity coefficient $\bar{\mu}_\mathrm{h} = K_\mathrm{v} K_\mathrm{e}$ is recovered as it should be.

Since expression (5) was derived from arguments of high Reynolds number turbulence (subscript h), the true average molecular viscosity is different near walls and at low Reynolds numbers. At a wall there are no velocity fluctuations, the flow is uni-directional, and the average viscosity must reduce to the pure viscometric form of Eq. (3), i.e. without any extensional effect.[2] To take this into account $\bar{\mu}_\mathrm{h}$ must be reduced by an appropriate molecular viscosity damping function f_v. Hence, the final expression for the average molecular viscosity $\bar{\mu}$ is

$$\bar{\mu} = f_v \bar{\mu}_\mathrm{h} + (1 - f_v)\eta_\mathrm{v}. \tag{8}$$

The role of f_v is akin to that of the damping function for the eddy viscosity f_μ and it was decided to make $f_v = f_\mu$ after an extensive series of tests analysed both the effects of $f_v > f_\mu$ and $f_v < f_\mu$ onto the predictions of the turbulence model. However, note that f_μ is not given by the standard Newtonian expression as it is affected by the new fluid rheology. Its new form is derived in Section 3.

2.2. The transport equations

Predictions in this paper are for fully-developed pipe flow of drag reducing fluids, hence the transport equations are simplified for this flow condition. The momentum equation to be solved is

$$0 = \frac{1}{r}\frac{\mathrm{d}}{\mathrm{d}r}\left[r\left(\bar{\mu}\frac{\mathrm{d}U}{\mathrm{d}r} - \rho\overline{uv}\right)\right] - \frac{\mathrm{d}\bar{p}}{\mathrm{d}x}, \tag{9}$$

where r is the radial coordinate, x the longitudinal coordinate, U the axial mean velocity and $\bar{p}$ the mean pressure.

The Reynolds shear stress is given by the turbulent viscosity hypothesis

$$-\rho\overline{uv} = \rho\nu_\mathrm{T}\frac{\partial U}{\partial r}, \tag{10}$$

where the eddy diffusivity ν_T is modelled by the Prandtl–Kolmogorov equation, modified by the damping function f_μ for low Reynolds number effects

$$\nu_\mathrm{T} = C_\mu f_\mu \frac{k^2}{\tilde{\varepsilon}}. \tag{11}$$

[2] $\dot{\varepsilon} = 0$ in 1D and 2D flows, see [10].

$\tilde{\varepsilon}$ is a modified rate of dissipation of turbulent kinetic energy used here, as in most near-wall low Reynolds number k–ε models [12], to facilitate the implementation of the wall boundary conditions. It is related to the true rate of dissipation ε by

$$\varepsilon = \tilde{\varepsilon} + D. \tag{12}$$

To determine k and ε two transport equations must be solved. For the viscoelastic fluids, the transport equation of k proposed by Pinho [10] is

$$0 = \frac{1}{r}\frac{\mathrm{d}}{\mathrm{d}r}\left[r\left(\frac{\bar{\mu}}{\rho} + \frac{\nu_\mathrm{T}}{\sigma_k}\right)\frac{\mathrm{d}k}{\mathrm{d}r}\right] + P_k - \tilde{\varepsilon} + D, \tag{13}$$

and the transport equation for $\tilde{\varepsilon}$ is

$$0 = \frac{1}{r}\frac{\mathrm{d}}{\mathrm{d}r}\left[r\left(\bar{\mu} + \rho\frac{\nu_\mathrm{T}}{\sigma_\varepsilon}\right)\frac{\mathrm{d}\tilde{\varepsilon}}{\mathrm{d}r}\right] + \rho f_1 C_{\varepsilon_1}\frac{\tilde{\varepsilon}}{k}P - \rho f_2 C_{\varepsilon_2}\frac{\tilde{\varepsilon}^2}{k} + E + C_{\varepsilon_4}\frac{\nu_\mathrm{T}}{\sigma_\mathrm{E}\bar{\nu}}\frac{\mathrm{d}\tilde{\varepsilon}}{\mathrm{d}r}\frac{\mathrm{d}\bar{\mu}}{\mathrm{d}r}. \tag{14}$$

In Eqs. (13) and (14) there are no convective terms on the left-hand side because of flow symmetry and fully-developed conditions. Similarly, the two new convective terms containing gradients of viscosity also vanish. In Eq. (13), P_k represents the production of turbulence kinetic energy and is given by

$$P_k = -\overline{uv}\frac{\partial U}{\partial r} = \nu_\mathrm{T}\left(\frac{\partial U}{\partial r}\right)^2. \tag{15}$$

This turbulence model has modifications relative to a Newtonian low Reynolds number k–ε model which are of two types:

(i) Direct changes due to a different constitutive equation, namely the addition of the last term on the right-hand side of the dissipation equation, the new time-average molecular viscosity and its damping function f_v. As will be shown, the effect of the new term in Eq. (14) is small.
(ii) Indirect modifications are new values and/or formulations for the existing numerical parameters and damping functions in the model. One example is the new form of the damping function f_μ resulting from the different constitutive equation. The more general expression derived here for f_μ includes the Newtonian damping function. The other damping functions and model parameters have not been changed and assume the forms and the numerical values used in Newtonian fluid mechanics. Further research is being carried out to ascertain their effects but in some cases results from new experiments are also required.

For Newtonian fluids there are many low Reynolds number k–ε models which differ in the form of the extra terms and damping functions [12,13]. Here, we start from the model proposed by Nagano and Hishida [14] which is modified for viscoelastic fluids. The model was chosen for its good performance in Newtonian pipe flow [14] and because its f_μ relied on Van Driest's function, a reasoning we also adopted to derive its new form as explained in the next section.

In Nagano and Hishida's model the various extra terms and damping functions are:

$$D = 2\bar{\nu}\left(\frac{\partial\sqrt{k}}{\partial r}\right)^2, \tag{16}$$

$$E = \bar{\nu}\nu_{\mathrm{T}}(1 - f_\mu)\left(\frac{\partial^2 U}{\partial r^2}\right)^2, \tag{17}$$

$$f_1 = 1.0, \tag{18}$$

$$f_2 = 1 - 0.3\exp(-R_{\mathrm{T}}^2). \tag{19}$$

For our purpose, these four equations are all modified, with the average molecular kinematic viscosity $\bar{\nu}$ ($\equiv\bar{\mu}/\rho$) taking the place of a constant kinematic viscosity. The damping function f_μ used by Nagano and Hishida [14] is given by the following equation:

$$f_\mu = \left[1 - \exp\left(-\frac{y^+}{26.5}\right)\right]^2, \tag{20}$$

where the wall coordinate y^+ (also called the wall Reynolds number) is given by Eq. (21). The damping function f_2 also needs the turbulence Reynolds number R_{T} defined by Eq. (22) which has also been modified by the use of $\bar{\nu}$. The viscosity appearing in Eq. (21) should be the wall viscosity ($\bar{\nu}_{\mathrm{w}}$) but a local viscosity ($\bar{\nu}$) will also be tested. To distinguish between both definitions of y^+, subscript w is used with the true wall coordinate of Eq. (23) but is omitted when using the local average molecular viscosity as in Eq. (21). u_τ stands for the friction velocity:

$$y^+ = \frac{u_\tau y}{\bar{\nu}}, \tag{21}$$

$$R_{\mathrm{T}} = \frac{k^2}{\bar{\nu}\tilde{\varepsilon}}, \tag{22}$$

$$y_{\mathrm{w}}^+ \equiv \frac{u_\tau y}{\bar{\nu}_{\mathrm{w}}}. \tag{23}$$

Note that the use of y_{w}^+ is common in the literature on non-Newtonian duct flows when representing near-wall data [15,16], although the subscript w is generally omitted.

The other coefficients, listed in Table 1, remain unchanged taking the Newtonian values because the experimental data required for their determination for viscoelastic fluids are scarce. Model parameters C_{ε_1} and C_{ε_2} require reliable high Reynolds number experiments in homogeneous shear flow and decay of grid-generated turbulence for viscoelastic fluids, respectively. For the former flow we are not aware of data whereas for the latter flow several works do not present sufficiently reliable information. Barnard and Sellin's [17] work on decay of turbulence is qualitative because it uses photography. The data of Greated [18] and McComb et al. [19] are not accurate enough (in [18] the decay of k for Newtonian fluids varies as a power of -1.9 when it should vary more like a power of -1.1). Still, using their data

Table 1
Values of the parameters assigned to Nagano and Hishida's low Reynolds k–ε model

C_μ	0.09
σ_k	1.0
σ_ε	1.3
C_{ε_1}	1.45
C_{ε_2}	1.90

(-1.9 for Newtonian and -1.5 for their 1000 wppm polyethylene oxide) would imply only a maximum increase in C_{ε_2} of 10% if C_{ε_3} is assumed to be zero. C_{ε_3} is the coefficient of a new convective term of the ε transport equation not present for fully-developed pipe or channel flow but appearing in the case of decay of grid-generated turbulence (Section 7 in [10]). Finally, the apparently more accurate experiments of Friehe and Schwarz [20] used hot-wire anemometry which is known to be an unreliable technique when dealing with polymer solutions.

Model parameter C_μ is usually quantified from experiments in oscillating grid turbulence but again no data for viscoelastic fluids are available, hence the standard Newtonian value of 0.09 is used. Determination of σ_ε is from data on wall turbulence but it depends on the values of C_{ε_1} and C_{ε_2} and now also on C_{ε_4}. For these reasons, and until there is better information on the homogeneous shear flow and decay of grid turbulence, it was decided to maintain the values of all these parameters identical to those used by Nagano and Hishida [14].

The determination of C_{ε_4} requires data from the same experiments as well as from an extra flow condition. Here, we are taking $C_{\varepsilon_4} = 1$ but further research is required to optimise this value.

3. The viscosity damping functions

In Sections 2.1 and 2.2 two damping functions were introduced for the viscosities: the molecular viscosity damping function f_ν and the eddy viscosity damping function f_μ. Both account for the inadequacies of the model to deal with low Reynolds number turbulence and in particular with wall blocking effects. They are different functions but in this work they were made identical after an extensive series of tests showed that $f_\nu \neq f_\mu$ resulted in less good predictions. This was assessed on the basis of friction factor versus Reynolds number data as well as by inspection of the radial profiles of various quantities. The equivalence of the two functions is unsurprising because both account for viscous effects on the total shear stress, although via different contributions.

3.1. The function f_μ

The damping function f_μ reduces the influence of the Reynolds shear stress on the total stress as the wall is approached, thus enhancing the influence of molecular viscosity. In the wall region, the purely viscous stress contribution dominates the total stress in the momentum balance. As pointed out by Patel et al. [12], in most low Reynolds number models f_μ was obtained by computer optimisation rather than by recourse to experimental data. One exception is the damping function of Nagano and Hishida [14] which is equivalent to the semi-empirical mixing length model proposed by Van Driest [21]. This is a possible reason for the superiority of Nagano and Hishida's model relative to other models in predicting pipe and channel flows and here it provides the possibility for a systematic procedure to derive an alternative damping function. These were the reasons for our choice of basic model: we wanted to concentrate on the specificities of drag reduction (DR) in pipe flow and so we selected a good model for Newtonian fluids to start with.

Function f_μ should be modified for consistency with the adopted rheological constitutive equation (Eqs. (2)–(4)) and for this purpose the philosophy used by Van Driest is used here.

Van Driest [21] assumed a similarity between the physics of the damping of turbulent eddies by a standing wall and the response of a fluid to the oscillation of a nearby plate under laminar flow conditions.

This laminar flow problem (Stokes' second problem) has a known solution where the amplitude of motion of the fluid varies according to $\exp(-y/A)$, with y representing the distance from the wall and parameter A depending on the frequency of oscillation of the plate and fluid properties. Since in turbulent flow the standing wall dampens fluid oscillations, Van Driest considered that the intensity of turbulent eddy motions should instead be proportional to the factor $1-\exp(-y/A)$. Subsequently, by using the mixing length hypothesis for the turbulent viscosity and by comparing predictions with experimental data, Van Driest refined his model, arriving at Eq. (20) after quantification of A.

To modify function f_μ accounting for the different fluid rheology, the same philosophy is used in our deduction. In the present case the drag reducing fluids have shear-thinning ($n < 1$) and Trouton-thickening ($p > 1$)[3] contributions, quantified by exponents n and p, respectively. As with the rheological model (Eq. (2)), the damping function adopted here is the product of a viscometric damping function $f_{\mu\mathrm{v}}$ by an elongational damping function $f_{\mu\mathrm{e}}$, i.e.

$$f_\mu = f_{\mu\mathrm{v}} f_{\mu\mathrm{e}}. \tag{24}$$

To derive functions $f_{\mu\mathrm{v}}$ and $f_{\mu\mathrm{e}}$ the philosophy of Van Driest is used separately for purely shear-thinning and purely Trouton-thickening fluids, respectively. To deduce $f_{\mu\mathrm{v}}$, Stokes' second problem for a power law fluid is analysed first with the aim of obtaining the law of variation with the wall distance y. This was done by Cruz et al. [22], but is summarised here because of its relevance to derive the expression for $f_{\mu\mathrm{e}}$ afterwards.

3.2. The viscometric damping function

In Stokes' second problem for a power law fluid, the momentum equation is given by

$$\frac{\partial u}{\partial t} = \frac{1}{Re_{\mathrm{ap}}}\frac{\partial}{\partial y}\left[\left|\frac{\partial u}{\partial y}\right|^{n-1}\left(\frac{\partial u}{\partial y}\right)\right], \quad y>0,\ t>0, \tag{25}$$

where Re_{ap} is an apparent Reynolds number (its exact definition is irrelevant for our purpose). The oscillating wall boundary condition is located at $y=0$ and is given by

$$u(t, y=0) = U_0\cos(\omega t). \tag{26}$$

The objective is not the complete solution to Stokes' second problem, but only the form of the expression quantifying the decay of fluid oscillations with distance from the wall $f(y)$. Then, the damping function for the turbulent eddies near a wall will be given by $1-f(y)$, according to Van Driest's reasoning.

Eq. (25) is solved with the following separation of variables:

$$u(t, y) = f(y)g(\phi) = f(y)g(\alpha_0 t + \alpha_1 \ln(f)), \tag{27}$$

where ϕ is a compounded variable and α_0 and α_1 are parameters. The following notation is used for conciseness:

$$f' \equiv \frac{\partial f}{\partial y} \quad \text{and} \quad g' \equiv \frac{\partial g}{\partial \phi}. \tag{28}$$

[3] Several authors hypothesise that drag reduction is related to a strain-thickening behaviour of the elongational viscosity η_{e}. In fact, what matters is the ratio $\eta_{\mathrm{e}}/\eta_{\mathrm{v}}$ and whether this quantity increases significantly beyond the theoretical value of 3 pertaining to purely viscous (inelastic) fluids. Here, such fluids are called Trouton-thickening.

Backsubstitution of these functions into Eq. (25) and after algebraic manipulation, the details of which can be found in [22], Eq. (25) becomes

$$\alpha_0 f g' = \frac{1}{Re_{\mathrm{ap}}}\left[n(g+\alpha_1 g')^n f''(f')^{n-1} + n\alpha_1(g+\alpha_1 g')^{n-1}(g'+\alpha_1 g'')\frac{(f')^{n+1}}{f}\right]. \tag{29}$$

Next, the solution we are looking for $f(y)$ is assumed to have the form

$$f(y) = (1+by)^r, \tag{30}$$

and, upon substitution on the right-hand side of Eq. (29) it becomes

$$\begin{aligned}\alpha_0 g'(1+by)^r = \frac{1}{Re_{\mathrm{ap}}}&[n(g+\alpha_1 g')^n r^n b^{n+1}(r-1)\\ &+ n\alpha_1(g+\alpha_1 g')^{n-1}(g'+\alpha_1 g'')r^{n+1}b^{n+1}][1+by]^{n(r-1)-1}.\end{aligned} \tag{31}$$

Both sides of this equation must depend identically on $[1+by]$, which requires

$$r = -\frac{1+n}{1-n}. \tag{32}$$

Now, function $f(y)$ is known, but has to be adapted to reproduce also the well-known exponential behaviour of Stokes' solution for Newtonian fluids as n approaches unity. Defining

$$b = b_0\left|\frac{1-n}{1+n}\right|, \tag{33}$$

where b_0 is a constant, $f(y)$ takes on the required form

$$f(y) = \left[1+\left|\frac{1-n}{1+n}\right| b_0 y\right]^{(1+n)/(1-n)}, \tag{34}$$

because an exponential is given by

$$\exp(-\beta) = \lim_{x\to 0}(1+\beta x)^{-1/x}. \tag{35}$$

By analogy with Van Driest's expression, the viscometric viscosity damping function for the turbulent eddies finally becomes

$$f_{\mu\mathrm{v}} = 1 - \left[1+\left|\frac{1-n}{1+n}\right| y^+\right]^{-|(1+n)/(1-n)|(1/A^+)}. \tag{36}$$

In the solution of Stokes' problem for a power law fluid, the definition of y^+ is obviously different from those in Eqs. (21) and (23). It depends on K_{v} and n in a way similar to that defined by Dodge and Metzner [23] which is

$$y^+_{\mathrm{DM}} \equiv \frac{\rho y^n u_\tau^{2-n}}{K_{\mathrm{v}}}. \tag{37}$$

For our purpose the use of both y^+ (Eq. (21)) and y^+_{w} (Eq. (23)) in $f_{\mu\mathrm{v}}$ will be tested, constituting what we call formulations M1 and M2 of the damping function, respectively. A constant parameter, introduced in the next section, accounts for discrepancies between predictions and experimental results.

3.3. The viscoelastic damping function

To deduce the viscoelastic damping function $f_{\mu e}$, which takes into account the wall blocking effect due to the Trouton ratio dependence of the viscosity ($p \neq 1$), a shear-independent fluid is considered ($n = 1$).

A derivation akin to that of the previous section is required, but for this purpose an expression relating the shear stress (τ) to the shear rate ($\dot{\gamma}$) is needed first. Since $n = 1$ such expression is obtained by order of magnitude arguments. Again, an exact solution to Stokes' second problem is not required, only its correct variation with wall distance is necessary.

The instantaneous rate of dissipation of turbulence kinetic energy for these non-Newtonian fluids has been defined by Pinho [10] as

$$\rho\hat{\varepsilon} \equiv 2\hat{\mu}s_{ij}^2. \tag{38}$$

The damping function is valid in the near-wall region where the flow is under equilibrium conditions $P_k = \varepsilon$, i.e.,

$$\rho\overline{uv}\frac{\partial u}{\partial y} \approx 2\eta_v K_e|\dot{\varepsilon}|^{p-1}\left(\frac{\partial u}{\partial y}\right)^2. \tag{39}$$

Here, the assumptions $s_{ij} \sim \partial u/\partial y$ and $U \sim u$ have been made for the near-wall region where U varies with y^+ and $\bar{u}'^2$ varies with $(y^+)^2$, see [13]. Small symbols are used to represent fluctuating quantities, capital letters or an overbar designate mean quantities and a hat is used to represent instantaneous quantities.

Solving in order to $\dot{\varepsilon}$ gives

$$\dot{\varepsilon} \approx \left[\frac{\rho\overline{uv}(\partial u/\partial y)^{p-2}}{2\eta_v K_e}\right]^{1/(p-1)}\frac{1}{\partial u/\partial y}. \tag{40}$$

In the near-wall region, the order of magnitude of $\overline{uv}(\partial u/\partial y)^{p-2}$ is estimated with:

$$\text{(i)}\ \ \mathrm{O}(\overline{uv}) \approx u_\tau^2,$$
$$\text{(ii)}\ \ \mathrm{O}\left(\frac{\partial u}{\partial y}\right) \approx \frac{u_\tau}{\bar{\nu}/u_\tau} = \frac{u_\tau^2}{\bar{\nu}}. \tag{41}$$

Backsubstituting yields

$$\dot{\varepsilon} \approx C\frac{u_\tau^2}{\partial u/\partial y}\left[\frac{\rho}{2\eta_v K_e \bar{\nu}^{p-2}}\right]^{1/(p-1)}, \tag{42}$$

where the calibration constant C has been introduced.

Now, substituting Eq. (42) into Eq. (2) with $n = 1$ gives, for the near-wall region,

$$\mu = \frac{\rho}{\bar{\nu}^{p-2}}(Cu_\tau^2)^{p-1}\left(\frac{\partial u}{\partial y}\right)^{1-p}, \tag{43}$$

or, in terms of shear stress, the fluid behaves according to

$$\tau = K_p\left(\frac{\partial u}{\partial y}\right)^{2-p} \quad \text{with } K_p = \frac{\rho}{\bar{\nu}^{p-2}}(Cu_\tau^2)^{p-1}. \tag{44}$$

With this power law expression equating the shear stress with the shear rate, the viscoelastic damping function can now be deduced in exactly the same way as the viscometric damping function of the previous

section, with $2-p$ taking the place of n. Hence, the viscoelastic damping function has a form in agreement with Eq. (36). However, the shear stress equation (44) also provides the definition of the wall coordinate to be used in $f_{\mu e}$. Within the viscous sublayer

$$K_p\left(\frac{\partial u}{\partial y}\right)^{2-p} = \rho u_\tau^2 \rightarrow \frac{\partial u}{\partial y} = \left(\frac{\rho u_\tau^2}{K_p}\right)^{1/(2-p)}, \tag{45}$$

so that using Eq. (44), and after integration of Eq. (45), the velocity is given by

$$\frac{u}{u_\tau} = \frac{y u_\tau}{\bar{\nu}} C^{(1-p)/(2-p)}. \tag{46}$$

The right-hand side of Eq. (46) is the wall coordinate for this specific solution and is the quantity that must be used in the viscoelastic contribution to the damping function. So, the viscoelastic damping function, taking into account the new definition of wall coordinate and the exponent $2-p$, is

$$f_{\mu e} = 1 - \left[1 + \left|\frac{p-1}{3-p}\right| y^+ C^{(1-p)/(2-p)}\right]^{-|(3-p)/(p-1)|(1/A^+)}, \tag{47}$$

which also reduces to Van Driest's expression as $p \rightarrow 1$ with $n = 1$.

Finally, the complete damping function f_μ is given by the following product:

$$f_\mu = \left\{1 - \left[1 + \left|\frac{1-n}{1+n}\right| y^+\right]^{-|(1+n)/(1-n)|/A^+}\right\}\left\{1 - \left[1 + \left|\frac{p-1}{3-p}\right| y^+ C^{(1-p)/(2-p)}\right]^{-|(3-p)/(p-1)|/A^+}\right\}. \tag{48}$$

Parameter A^+ takes the value of 26.5 used by Nagano and Hishida, which is very close to the Van Driest value, and parameter C is obtained by fitting predictions to experiments, the subject of Section 4.1.

4. Results and discussion

To test the turbulence model its predictions must be compared with sets of experimental data that include measurements of the viscometric and extensional viscosities as well as with data for purely shear-thinning fluids with no elasticity. If data on the viscometric viscosity are easy to obtain and are usually included with the hydrodynamic results, the measurement of extensional viscosity is difficult, especially for very mobile systems, and so very few data are available.

Difficulties at measuring the extensional viscosity are well known by those in the field of polymer processing [24]. Major improvements have taken place over the last 10 years so that there are currently reliable techniques for probing polymer melts and concentrated solutions and providing accurate and reproducible results [25]. However, for low consistency fluids the measurement of extensional viscosity is far more difficult [26]. One of the techniques to measure a property related to the extensional viscosity for very dilute fluids is the opposed-jet rheometer developed by Fuller et al. [27]. In spite of its shortcomings [28], it still remains one of the best methods for dilute polymer solutions.

Simultaneous measurements of extensional viscosity and hydrodynamic quantities for dilute polymer solutions are not abundant. To our knowledge there are only two works where such measurements have been carried out as part of a broader experimental research on DR in turbulent pipe flow: Escudier et al.

Table 2
Parameters of viscosity law of Eqs. (2)–(4) used to fit the viscosity data in [9]

Fluid	K_v (Pa s^n)	n	K_e	p
0.25% CMC	0.2639	0.6174	2.0760	1.2678
0.3% CMC	0.2748	0.6377	2.7485	1.2214
0.4% CMC	0.2528	0.6177	0.9283	1.3982
0.09/0.09% CMC/XG	0.15178	0.5783	2.1833	1.1638
0.2% XG	0.2701	0.4409	3.8519	1.2592
0.125% PAA	0.2491	0.425	1.9394	1.4796
0.2% PAA	0.7849	0.4075	9.865	1.3175

[9] and Presti [29]. These two sources of experimental data are the basis of comparisons in this paper for drag reducing fluids. For purely shear-thinning inelastic fluids the comparisons are made in relation to the correlations of Dodge and Metzner [23] and the numerical data of Malin [30]. More details of these works are presented later.

Escudier et al. [9] performed measurements of pressure drop, flow rate and radial profiles of mean velocity using LDA. Their pipe had a diameter of 100.4 mm and their fluids were aqueous solutions of polyacrylamide (PAA), xanthan gum (XG), carboxymethyl cellulose (CMC) and a blend of XG and CMC at various weight concentrations. The rheological measurements include data on the viscometric viscosity, first normal stress difference and especially on the elongational viscosity, the property that the present turbulence model uses in a specific way to mimic viscoelastic effects. The corresponding turbulence kinetic energy data are available in [29].

Fitting Eqs. (3) and (4) to the viscometric and extensional viscosity data in [9], yielded the parameters listed in Table 2.

All solutions are shear-thinning and Trouton-thickening, i.e., although the extensional viscosity was found to be strain-thinning, its rate of decrease with strain rate is slower than that of the viscometric viscosity with shear rate and consequently the Trouton ratio increases with the rate of deformation of the fluid.

First, a series of simulations is carried out with the aqueous solution of 0.125% PAA, aimed at determining the value of parameter C appearing in the damping function $f_{\mu e}$. This fluid was selected randomly. Then, using only the flow rate and the rheology of the fluids as input conditions, predictions of turbulent flow for other fluids were performed. Predictions were also carried out for pure shear-thinning and pure Trouton-thickening fluids to assess the behaviour of the turbulence model under these two limiting conditions. For the former case comparisons can be made with correlations from the literature.

The numerical simulations were carried out with a finite volume code developed by Younis [31] for boundary layer flows. The code was adequately modified for the viscoelastic fluids and the current turbulence model. The non-uniform mesh used had 199 cells from wall to wall and had at least 12 control volumes within each viscous sublayer ($y_w^+ < 5$). This mesh was selected after a preliminary investigation for Newtonian and non-Newtonian fluids showed that the grid provided mesh-independent results within 0.1%.

4.1. Determination of parameter C

The correct strategy for evaluating parameter C would be the solution of an inverse problem, but this was not attempted and a trial-and-error method was used instead. Using the rheology for 0.125% PAA several

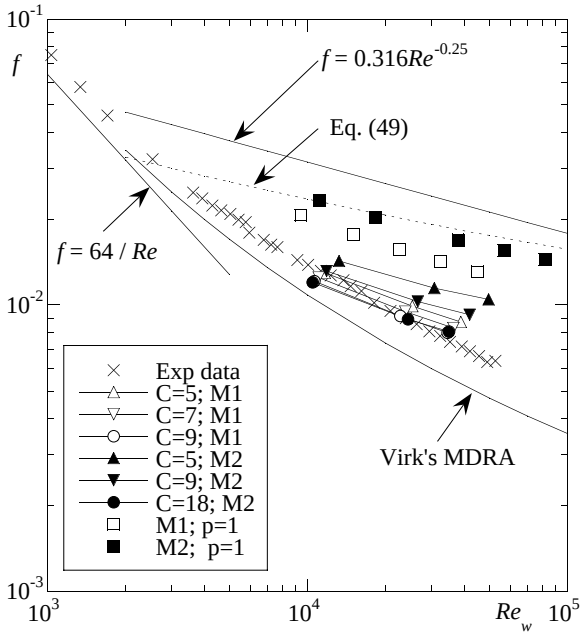

Fig. 1. Comparison between the predicted and experimental [9] fRe for 0.125% PAA. Open symbols (M1) refer to Model 1, closed symbols (M2) refer to Model 2. $p = 1$ refers to simulations for purely viscous 0.125% PAA solution.

numerical values of C were tried and the predictions of $f - Re_w$ were compared with the experimental $f - Re_w$ data, where f is Darcy's friction coefficient and Re_w the Reynolds number based on the wall viscosity and bulk flow velocity. This Reynolds number is used throughout the paper.

Fig. 1 compares the predictions of $f - Re_w$ with data from Escudier et al. [9]. The computations were made with formulations M1 and M2 of the damping function. M2 gave higher values of the friction coefficient than M1, but in both cases the amount of DR was clearly in excess to that due to purely shear-thinning behaviour represented by the dashed line. The dashed line represents the friction factor for a purely viscous fluid ($K_e = 1$, $p = 1$) obeying the same power law model as the 0.125% PAA fluid ($n = 0.425$) according to Eq. (49) derived from Dodge and Metzner [23]. For reference, the maximum DR asymptote of Virk et al. (MDRA) [32] given by Eq. (50), is also plotted:

$$\frac{1}{\sqrt{f}} = 0.8685 n^{0.25} \ln\left(\frac{2n}{3n+1} Re_w \sqrt{f}\right) + \frac{2.4082}{n^{0.75}}(1-n) - \frac{0.2}{n^{1.2}}, \tag{49}$$

$$\frac{1}{\sqrt{f}} = 9.5 \log(Re_w \sqrt{f}) - 19.06. \tag{50}$$

For the predictions to compare well with experimental data a value of $C = 9$ is needed together with formulation M1. For M2 a higher value of C (=18) is required to approach predictions and experimental data, especially at high Reynolds numbers. Parameter C was introduced in the order of magnitude analysis leading to $f_{\mu e}$ and in principle it should not differ from 1 by more than a factor of 10, otherwise the order of magnitude analysis would be grossly in error. In what follows $C = 9$ for both damping functions, but results are also presented using $C = 18$ for M2.

The slope of the $f - Re_w$ predictions are less than that for the measurements indicating the need for further improvements in the turbulence model. The figure includes results of simulations for a similar fluid without strain-rate dependence of the Trouton ratio ($p = 1$). For formulation M2, the predictions compare well with Eq. (49) showing no elastic DR as it should: at Reynolds numbers of the order of 10,000 the difference relative to Eq. (49) is of the order of 1% or less whereas at high Reynolds numbers the model predicts a lower value of f by about 10%. At lower Reynolds numbers the model predicts higher values of f, the difference never exceeding 10%. In contrast, formulation M1 predicts excessive DR for pure shear-thinning fluids and this is a first indication that the M2 formulation of the damping function is to be preferred, in spite of a less good prediction of the friction factor for viscoelastic fluids. Further evidence of the advantages of model M2 will appear later. Note that with $p = 1$ the numerical value of C is irrelevant.

The disagreement between the experimental data and the laminar correlation at low Reynolds numbers ($f\,Re = 64$) is due to different Reynolds number definitions. The data are plotted here using the wall Reynolds number, whereas the correlation $f = 64/Re$ is only universal when using the generalised Reynolds number. Still, the laminar theoretical expression is plotted to help read the graph.

Next, the behaviour of turbulence models M1 and M2 are assessed by comparing their results for other fluids with the corresponding experimental data in terms of $f - Re_w$ and other relevant quantities. Predictions by model M2 are also investigated for inelastic shear-thinning fluids and purely Trouton-thickening fluids, i.e. fluids devoid of shear-thinning.

4.2. Other predictions of friction factor

4.2.1. Drag reducing fluids

Using $C = 9$ for M1 and M2 and $C = 18$ for M2, predictions for several of the remaining experimental data sets of Escudier et al. [9] were carried out and the friction factor data are compared in Fig. 2. In Section 4.3.1, the corresponding velocity profiles are plotted.

Fig. 2 shows mixed results: with $C = 9$ formulation M2 results in less DR than M1, but the difference is particularly large for the 0.2% XG solution (in excess of 30%) and less so for the blend of CMC and XG (20%). With the other fluids the predictions of DR with Model 2 are about 15% lower than those obtained by Model 1. Increasing C to 18 helps in that the values of f decrease and are in between those for $C = 9$ with M1 and M2 and closer to experimental data. Note that the DR is given by

$$\text{DR}\,(\%) = \frac{f - f_N}{f_N} \times 100, \tag{51}$$

where f_N is the Newtonian friction factor at identical wall Reynolds number. Of significance is the fact that in all predictions the DR was significantly larger than the amount exclusively attributed to shear-thinning, the latter given by Eq. (49).

M1 predicted well the results for 0.25% CMC and the blend (at low Reynolds numbers) and slightly overestimates DR for the 0.3 and 0.4% CMC solutions. M2 with $C = 9$ predicted well the DR for 0.3 and 0.25% CMC at low Reynolds numbers, over predicted DR for 0.4% CMC and under predicted in the other cases. M2 with $C = 18$ predicted well for 0.25 and 0.3% CMC, but now over a wider range of Reynolds numbers, also over predicted 0.4% CMC and for the blend, the improvement in f was small.

Regardless of the turbulence model, in all cases the slopes of predicted $f - Re_w$ were lower than the slopes of the measured $f - Re_w$ data, hence the agreement between predictions and experiments is always

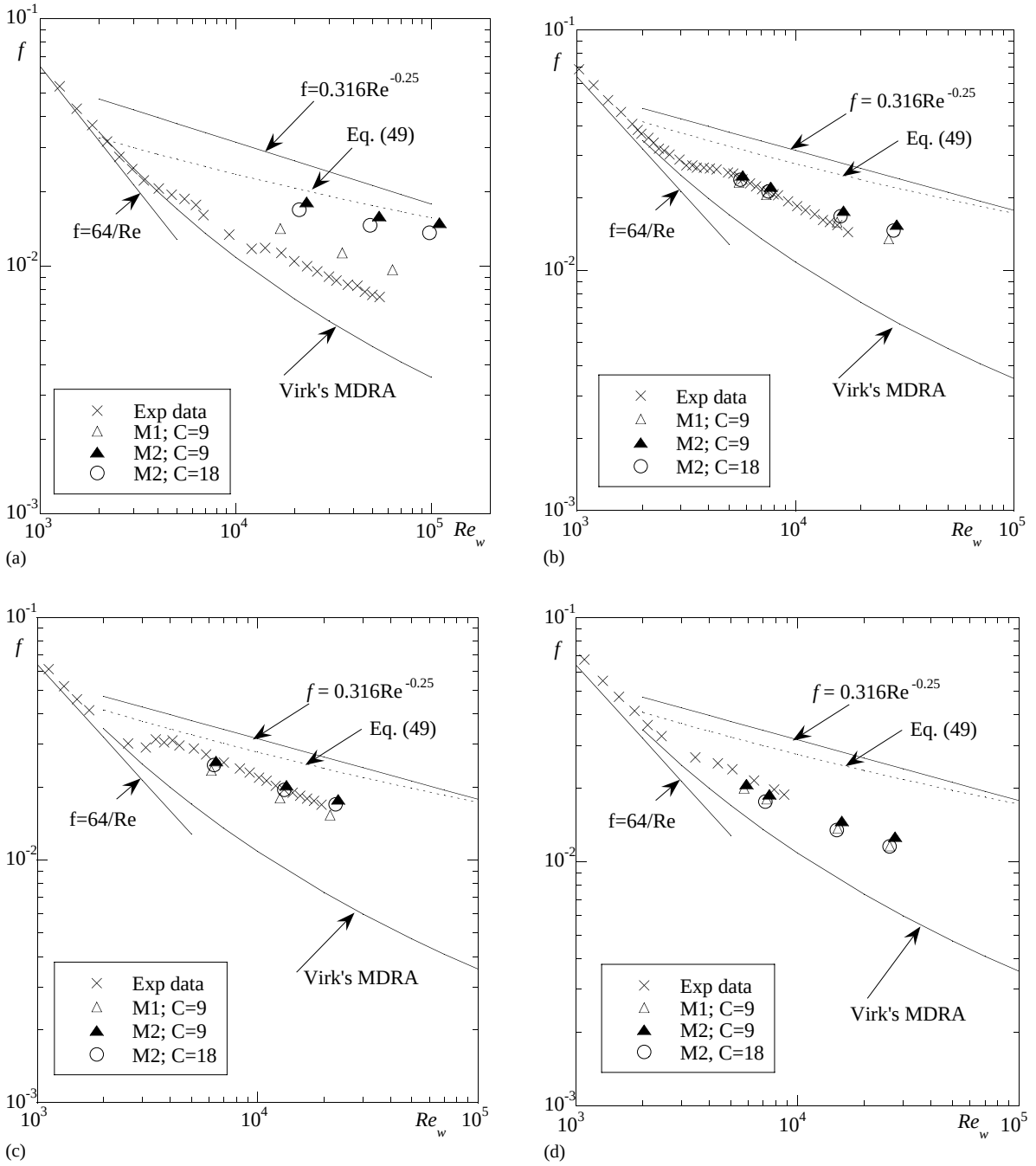

Fig. 2. Comparison between predicted and measured fRe [9] for various polymer solutions: (a) 0.2% XG; (b) 0.25% CMC; (c) 0.3% CMC; (d) 0.4% CMC; (e) 0.09/0.09% CMC/XG blend; (f) 0.2% PAA.

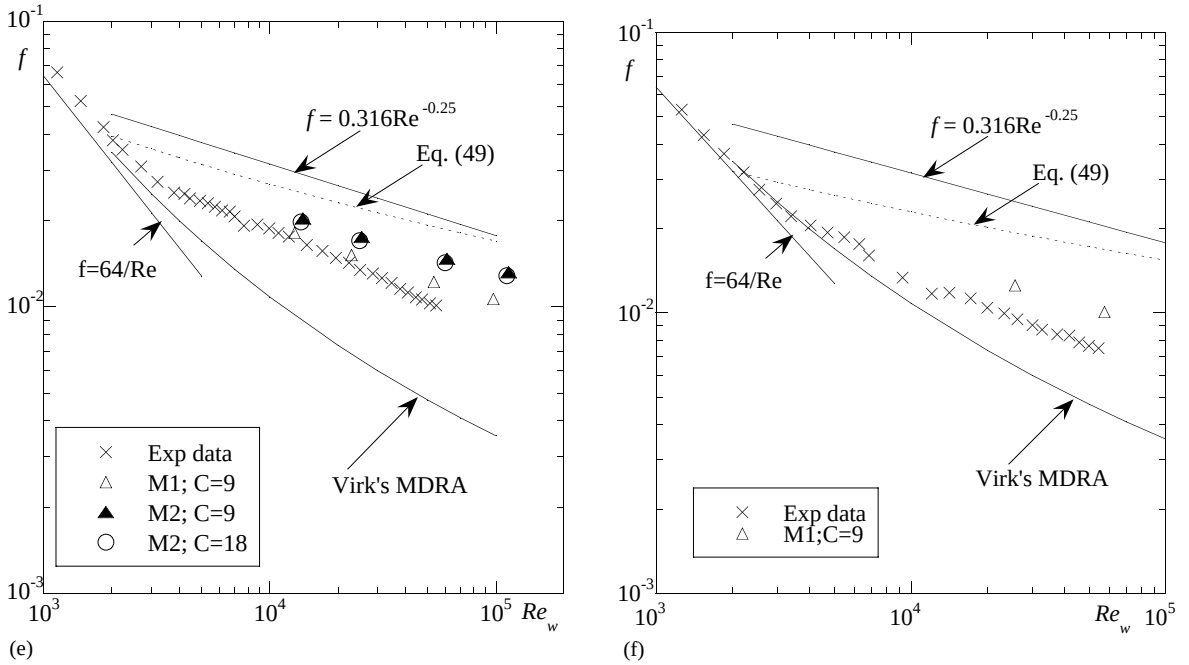

Fig. 2. (*Continued*).

over a limited range of Reynolds numbers. Still, it is important to emphasise that this is the first time a general turbulence model, not previously tuned with the flows to be predicted, has been able to calculate such intense DRs in turbulent viscoelastic pipe flow.

For the 0.2% PAA solution there were numerical difficulties in obtaining converged solutions at low Reynolds number flows comparable to those of the experiments, especially when using formulation M2.

4.2.2. Inelastic shear-thinning fluids

Dodge and Metzner [23] semi-empirically derived expressions for the friction factor and the mean velocity profile in turbulent pipe flow of power law fluids. These are still accepted today as representative of the behaviour of fluids devoid of any elasticity although the fluids used to quantify the parameters by Dodge and Metzner included a few polymer solutions that could be weakly elastic.

The present turbulence model should behave well for purely viscous shear-thinning fluids ($K_e = 1$, $p = 1$) and in Fig. 3 comparisons of the predicted $f - Re_g$ data are made with the original correlation of Dodge and Metzner (Eq. (52)) except that the friction factor plotted is the Darcy coefficient rather than the Fanning factor in [23]. The generalised Reynolds number defined in Eq. (53) is used in the plot and in Eq. (52). The dashed line represents the smooth pipe Blasius equation (54):

$$\frac{1}{\sqrt{f_F}} = \frac{4}{n^{0.75}} \log[Re_g (f_F)^{(2-n)/2}] - \frac{0.4}{n^{1.2}}, \tag{52}$$

$$Re_g = \frac{\rho U^{2-n} D^n}{K_v 8^{n-1} [(3n+1)/4n]^n}, \tag{53}$$

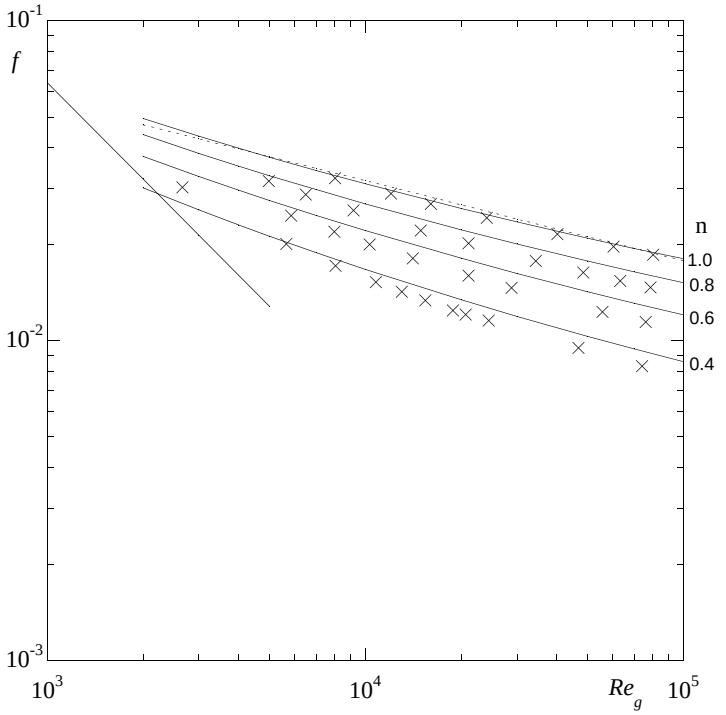

Fig. 3. Comparison between predicted and the correlation of Dodge and Metzner [23] (Eq. (52)) for the friction factor of purely viscous shear-thinning fluids.

$$f = 0.316\,Re^{-1/4}. \tag{54}$$

The predictions in Fig. 3 were obtained with the M2 formulation and the plot shows that the model underestimates the friction factor by 10% at high Reynolds numbers. At very low Reynolds numbers, the predicted f tends to be higher than the correlation.

In 1997 Malin [30] developed a low Reynolds number k–ε turbulence model exclusively for purely viscous power law fluids. His model was based on the Lam–Bremhorst's [33] damping function which he modified empirically by including the power index n but he gave no account of any effects of the non-linear non-Newtonian viscosity on the turbulence model, except for the consideration of the power viscosity law for molecular diffusion terms. For strongly shear-thinning fluids ($n = 0.4$) our predictions are of similar quality as theirs but for weakly shear-thinning intensities their predictions of f are closer to the correlation than ours, except for $n = 1$ where we have much better agreement. However, whereas our model can predict the behaviour of elastic fluids, Malin's model only works for purely viscous fluids. Note also that, and in contrast to Malin, no attempts have been made in this work to tune the constants of the turbulence model in order to improve its predictions for purely viscous fluids.

4.2.3. Trouton ratio thickening fluids

For fluids of constant shear viscosity with different degrees of strain-hardening of the extensional viscosity, predictions were also carried out using $C = 9$ and 18 and results of $f - Re$ are shown in Fig. 4. As the exponent p is raised the DR increases and for a value of p of around 1.7 and $C = 9$ the values of f

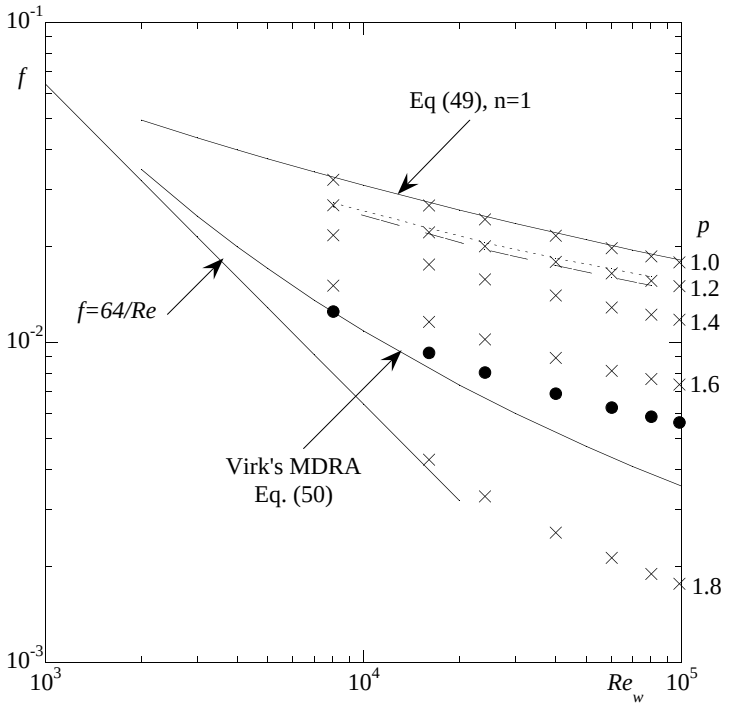

Fig. 4. Effect of Trouton ratio hardening exponent p on predictions of $f - Re$ for constant shear viscosity fluids ($n = 1$) and formulation M2. Symbols: $K_e = 1$ (crosses: $C = 9$, black circle: $p = 1.6$, $C = 18$); short dashed line: $K_e = 2$, $p = 1.2$, $C = 9$; long dashed line: $K_e = 0.5$, $p = 1.2$, $C = 9$.

will fall in the vicinity of Virk's MDRA asymptote. These predictions were obtained with the formulation M2 of the damping function f_μ which was seen to lead to higher values of f than the more drag reducing M1 formulation. With $C = 18$ the friction factor is lower, other parameters being equal, so at very low Reynolds numbers the predictions collapse already with Virk's asymptote. Note that $C = 18$ was the optimised value for the M2 formulation with which all predictions in Fig. 4 were carried out.

In conclusion, the present model is capable of predicting very high DRs for constant shear viscosity fluids, a feature than has been observed experimentally many times but this requires intense strain-hardening of the Trouton ratio.

The model is far less sensitive to K_e and this is also shown in Fig. 4. For $p = 1.2$ simulations were also carried out for $K_e = 0.5$ and 2 and these are represented as long dashed and short dashed lines, respectively. Now, the friction factor is proportional to K_e but the effect is small in comparison to the effect of p.

4.3. Mean velocity

4.3.1. Drag reducing fluids

Figs. 5–8 compare predicted mean velocity profiles in wall coordinates with measured data from Escudier et al. [9]. Other cases are not shown here for conciseness, but the comparisons are qualitatively identical.

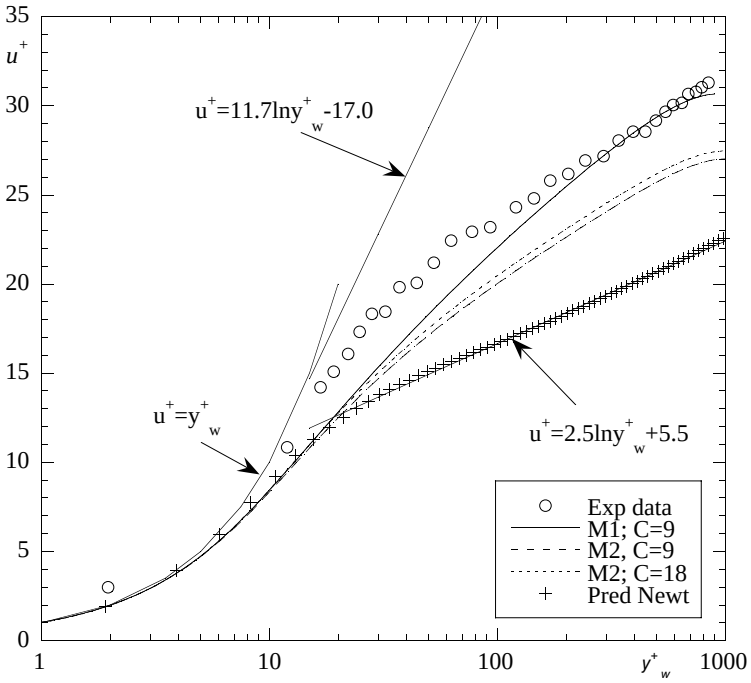

Fig. 5. Comparison between calculated and experimental ($Re_w = 45{,}300$ [9]) velocity profiles in wall coordinates for the 0.09/0.09% CMC/XG solution. The figure includes the Newtonian prediction at $Re_w = 200{,}800$ using the same code (+).

These figures include several velocity curves: the Newtonian log-law, the viscous sublayer velocity profile and Virk's ultimate DR asymptote [34]. Fig. 5 also includes predictions for a Newtonian fluid at a high Reynolds number of 200,080. This Newtonian prediction was obtained with this same model and code by setting n and p equal to 1: the predicted profile collapses with the viscous sublayer equation for $y_w^+ < 4$ and is in agreement with a standard Newtonian log-law expression for $y_w^+ > 40$, thus confirming the generality of the proposed turbulence model.

The experimental velocity profiles show basically three regions in agreement with Virk [34]: the viscous sublayer at low values of y_w^+, an inertial layer with almost the same slope as the Newtonian log-law at high y_w^+, and an intermediate log layer with a high slope. So, outside the viscous sublayer, say for $y_w^+ > 10$, the experimental data show two regions of linear behaviour in a semi-log plot, except for very large DRs when the intermediate log-law occupies the whole pipe.

The comparisons between the non-Newtonian predictions and the experiments are remarkable considering the novelty of the turbulence model. As expected, the turbulence model captures the viscous sublayer and then results in a log-law having a higher slope than the Newtonian log-law except at the pipe centre where the velocity becomes constant. This behaviour is qualitatively in agreement with the experiments although some of the features are not seen in these plots. In particular, the predictions do not show the double log-law behaviour outside the viscous sublayer. Predictions with M1 are closer to Virk's asymptote than those of M2 as with the friction factor data and consistent are also the predictions for M2 with $C = 18$ standing in between those for M1 and M2 with $C = 9$. In this respect, the exception is the behaviour for 0.125% PAA as explained next.

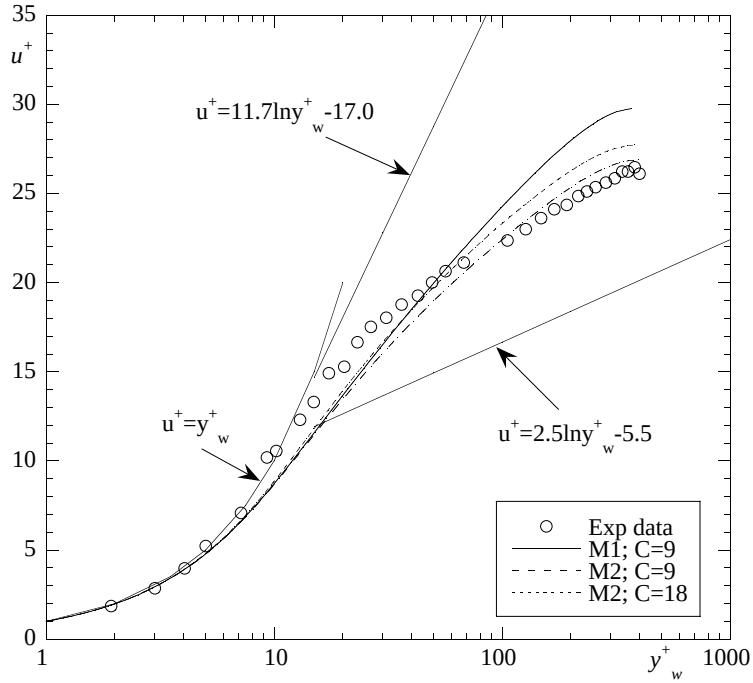

Fig. 6. Comparison between calculated and experimental ($Re_w = 16{,}600$ [9]) velocity profiles in wall coordinates for the 0.25% CMC solution.

In none of the predicted cases the velocity profile coincides with Virk's asymptote especially for the 0.125% PAA in Fig. 8: here, whereas the experimental data collapse onto Virk's asymptote, the predicted velocities do not but are not too far, especially for M2 with $C = 18$ and M1. In contrast to the other cases here it is the prediction by M2 with $C = 18$ that is closer to the experimental data although in terms of $f - Re_w$ both predictions are equivalent because $f - Re_w$ for 0.125% PAA was the case used to quantify parameter C (see Fig. 1). It is also interesting to notice that although the experimental velocity data coincide with Virk's MDRA, the experimental friction factor data do not, i.e., the numerical friction factor and velocity data seem to be more consistent than the experimental f and velocity data and here it is the M2 with $C = 18$ that is closer to the experimental results.

In some cases, the predictions are in between the experimental data, i.e., at low y_w^+ the experimental velocities are under predicted whereas at high y_w^+ they are over predicted as for the 0.3% CMC solution. For 0.25% CMC the velocity prediction by M2 with $C = 18$ is better than those of M1 and M2 ($C = 9$) whereas for the blend M1 is better. For the 0.3% CMC solution the velocity prediction by M2 with $C = 9$ is better but still far from following the trend of the experiments at high y_w^+.

In our opinion, the absence of the inertial log-law at high y_w^+ for the flows with less DR could be related either to the absence of a region where the damping function assumes a constant value or to the low Reynolds numbers of the flows tested here.

4.3.2. Inelastic shear-thinning fluids

Predicted velocity profiles in wall coordinates are compared in Fig. 9 with correlations from the literature. All the numerical simulations in Fig. 9 correspond to $Re_g = 40{,}000$, the flow condition used

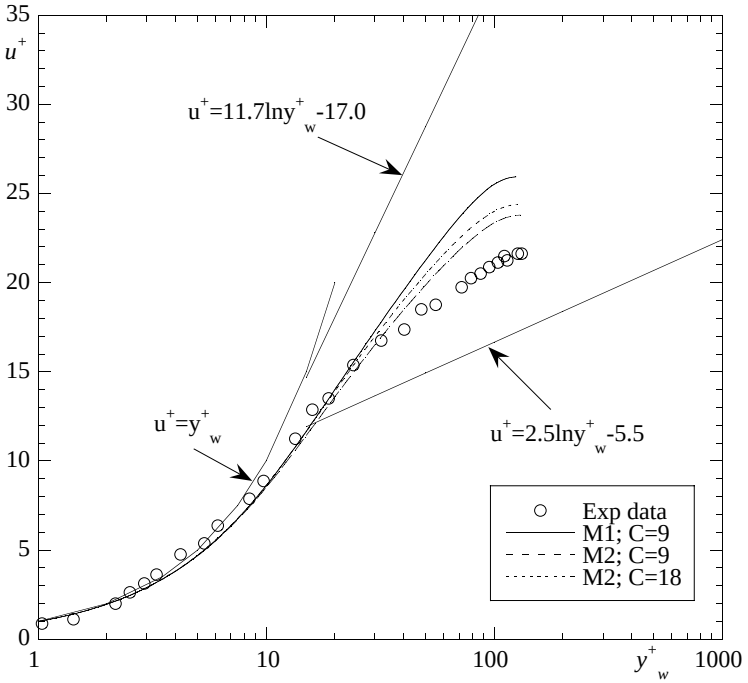

Fig. 7. Comparison between calculated and experimental ($Re_w = 4300$ [9]) velocity profiles in wall coordinates for the 0.3% CMC solution.

by Malin [30]. In Fig. 9(a), the wall coordinate is that proposed by Dodge and Metzner [23] (y^+_{DM}) and defined in Eq. (37), whereas in Fig. 9(b) the wall viscosity (Eq. (23)) is used instead.

In the viscous sublayer the predictions collapse onto the corresponding theoretical expressions (Eq. (55)). In the inertial sublayer the equation provided by Dodge and Metzner [23] is wrong, as pointed out by Skelland [35] who corrected their expression (Eq. (6.68) in [35]) here transcribed as Eq. (56a) and plotted in Fig. 9(a). The predicted velocities are slightly above Eq. (56a) and this is consistent with Fig. 3 where the predicted friction factors are slightly below the corresponding expression from Dodge and Metzner [23]:

$$u^+ = (y^+_{DM})^{1/n}, \tag{55a}$$

$$u^+ = y^+_w, \tag{55b}$$

$$u^+ = \frac{5.657}{n^{0.75}} \log y^+_{DM} - \frac{0.566}{n^{1.2}} + \frac{3.475}{n^{0.75}} \left[1.96 + 0.816n - 1.628n \log\left(3 + \frac{1}{n}\right) \right], \tag{56a}$$

$$u^+ = 5.657 n^{0.25} \log y^+_w - \frac{0.566}{n^{1.2}} + \frac{3.475}{n^{0.75}} \left[1.96 + 0.816n - 1.628n \log\left(3 + \frac{1}{n}\right) \right]. \tag{56b}$$

The corresponding plot using wall coordinates based on the wall viscosity in Fig. 9(b) shows a better agreement of predictions with Eq. (56b) which is equivalent to Eq. (56a) using y^+_w.

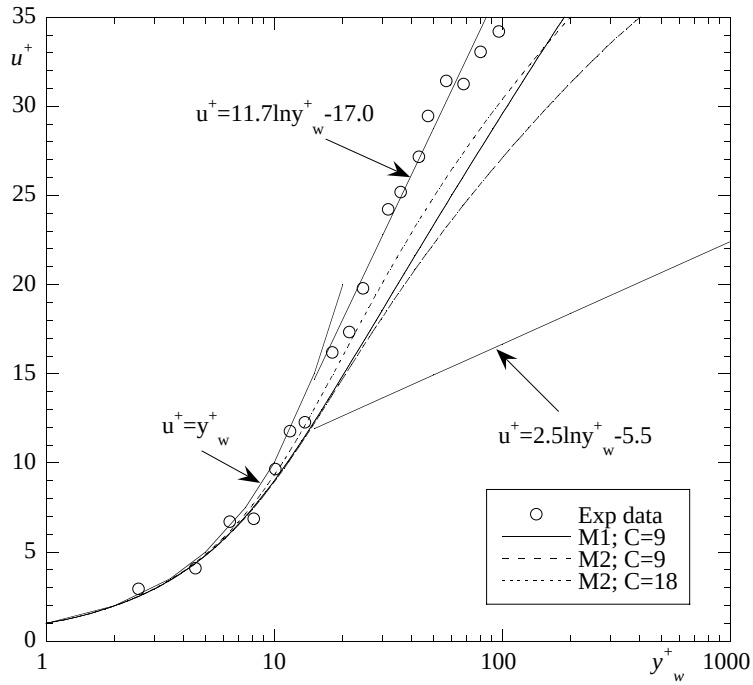

Fig. 8. Comparison between calculated and experimental ($Re_w = 42{,}900$ [9]) velocity profiles in wall coordinates for the 0.125% PAA solution.

The level of agreement between our predictions and the correlations from the literature is similar to that reported by Malin [30]. Note, however, that although Malin compared the friction factor with Dodge and Metzner's expression for f, he did not compare his velocity profiles with Skelland's corrected profile and instead used a non-universal correlation.

4.3.3. Trouton ratio thickening fluids

The effect of strain-hardening of the extensional viscosity on predictions of the velocity profile for constant shear viscosity fluids is shown in Fig. 10. In agreement with the $f - Re$ behaviour of Fig. 4, as p increases the velocity profile shifts positively from the Newtonian inertial sublayer towards Virk's asymptote (Eq. (57)) and exceeds it as for $p = 1.8$ the data of which are close to that for laminar flow. The results of both Figs. 4 and 10 are clearly consistent and suggest that Virk's asymptotes for friction factor and velocity are reached for p of around 1.7:

$$u^+ = 11.7 \ln y_w^+ - 17.0. \tag{57}$$

If C is set equal to 18, the optimised value of C for formulation M2, the velocity profile for $p = 1.6$ is closer to Virk's asymptote than the profile for $C = 9$. Also, for $y_w^+ < 50$ there is agreement between predictions and Virk's MDRA. Another important finding from this plot is that here the velocity profiles do show the three layers identified by Virk [34]. For $p = 1.6$ (regardless of C) the plot shows that the predicted profile follows the viscous sublayer very close to the wall, followed by the intermediate sublayer and far from the wall a shifted log-law with the same slope as the Newtonian log-law. This

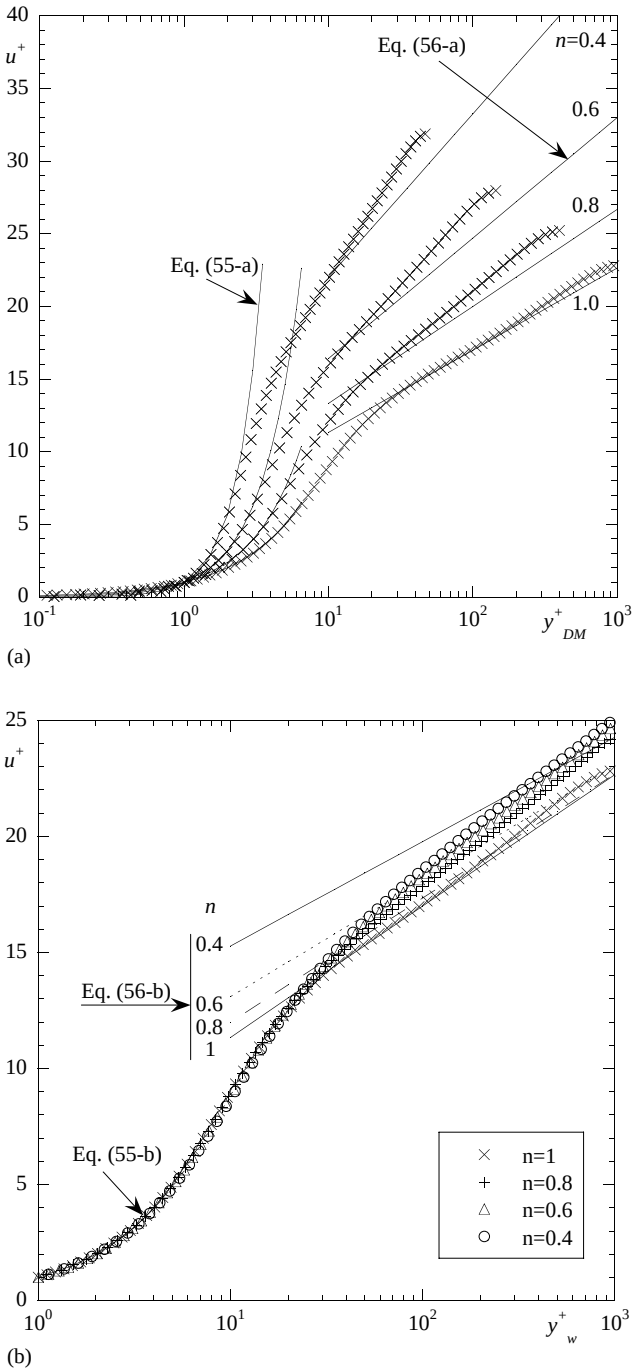

Fig. 9. Comparison between predicted (model M2) and the profile of Skelland [35] (Eq. (57)) for the velocity profile in wall coordinates of purely viscous shear-thinning fluids. Dashed lines represent viscous sublayer; solid lines represent inertial layer: (a) $u^+ - y^+_{DM}$ plot; (b) $u^+ - y^+_w$ plot.

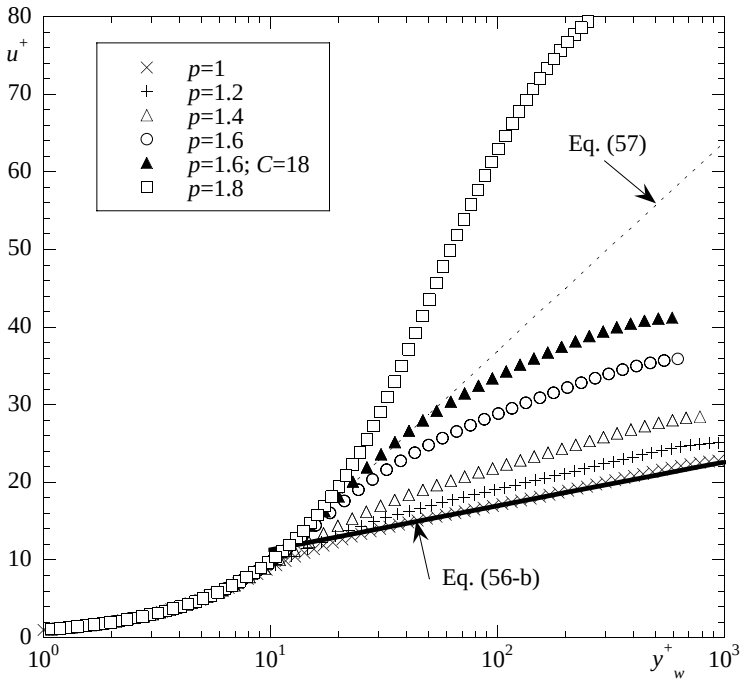

Fig. 10. Effect of Trouton ratio hardening exponent p on predictions of the velocity profile in wall coordinates for constant shear viscosity fluids ($n = 1$, $C = 9$), formulation M2 and $Re_w = 40{,}000$.

supports our argument in Section 4.3.1 that the absence of the shifted inertial layer could be caused by the low Reynolds number of the simulations there and should not be immediately considered as a defect of the present closure.

4.4. Turbulent kinetic energy

4.4.1. Drag reducing fluids

Predicted profiles of turbulence kinetic energies are compared with experimental data from Presti [29] in Figs. 11–14. Each plot includes data obtained with formulations M1 and M2 with $C = 9$ and M2 with $C = 18$ and the results are presented both in wall and physical coordinates. The data from Presti [29] correspond to the same flow conditions as the mean flow data of Escudier et al. [9].

In general, the turbulence models over predict turbulence in the central region of the pipe, and in the wall layer the peak turbulence is over predicted in M1 and under predicted in M2, except for the PAA in physical coordinates (Fig. 14). The experiments show that the peak turbulence for drag reducing fluids is always higher than for Newtonian fluids but it is located farther away from the wall, especially when viewed in wall coordinates. These features are also captured by the predictions although by different amounts in relation to the experimental data and in several cases the turbulence in the pipe core is well predicted by formulation M2 (the blend, 0.2% XG and 0.125% PAA solutions). As far as the location of the peak turbulence is concerned, it is usually over predicted, except for the blend in physical coordinates. In the inertial layer k^+ is well predicted by formulation M2 for the high Reynolds number cases: XG, the

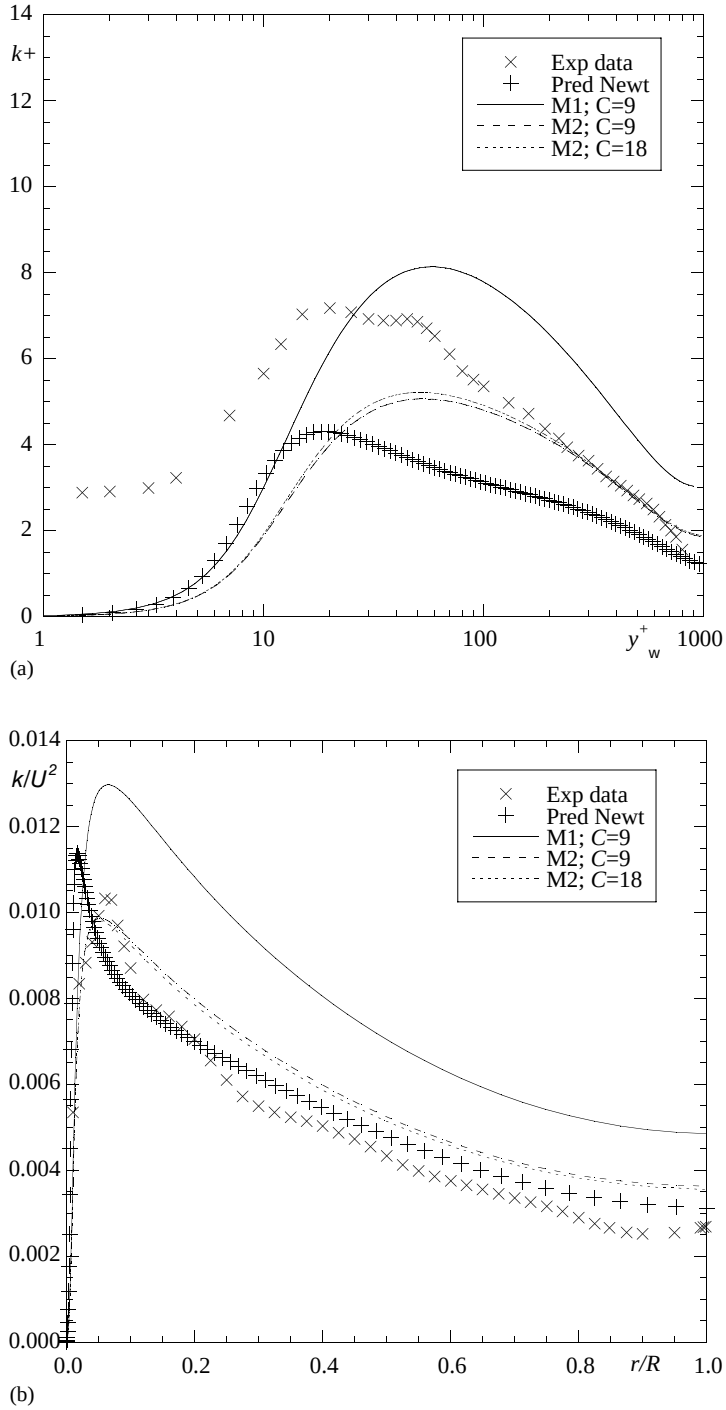

Fig. 11. Comparison between calculated ($Re_w = 45{,}300$) and experimental ($Re_w = 45{,}300$ [29]) profiles of turbulence kinetic energy for the blend of 0.09/0.09% CMC/XG: (a) wall normalisation; (b) physical normalisation; for water $Re_w = 42{,}970$.

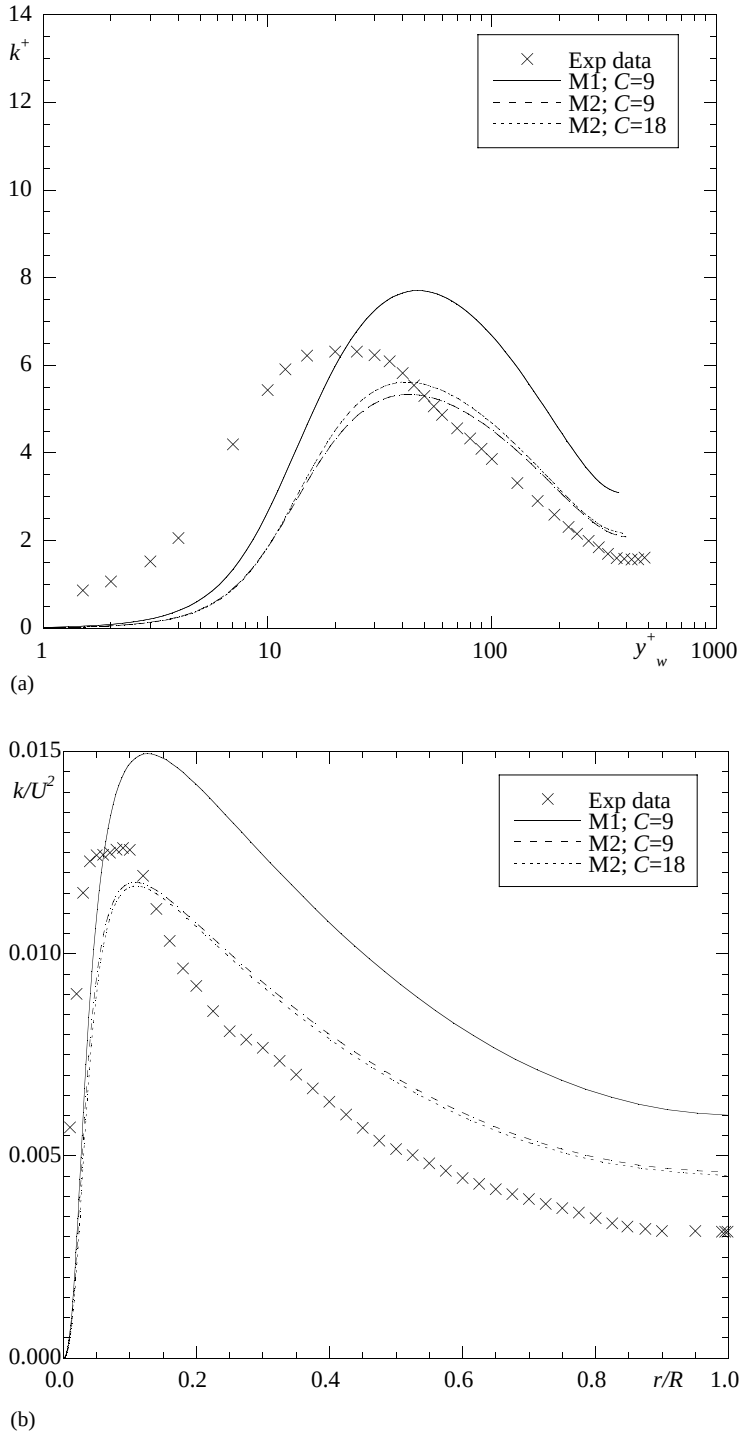

Fig. 12. Comparison between calculated ($Re_w = 16{,}280$) and experimental ($Re_w = 16{,}600$ [29]) profiles of turbulence kinetic energy for 0.25% CMC solution: (a) wall normalisation; (b) physical normalisation.

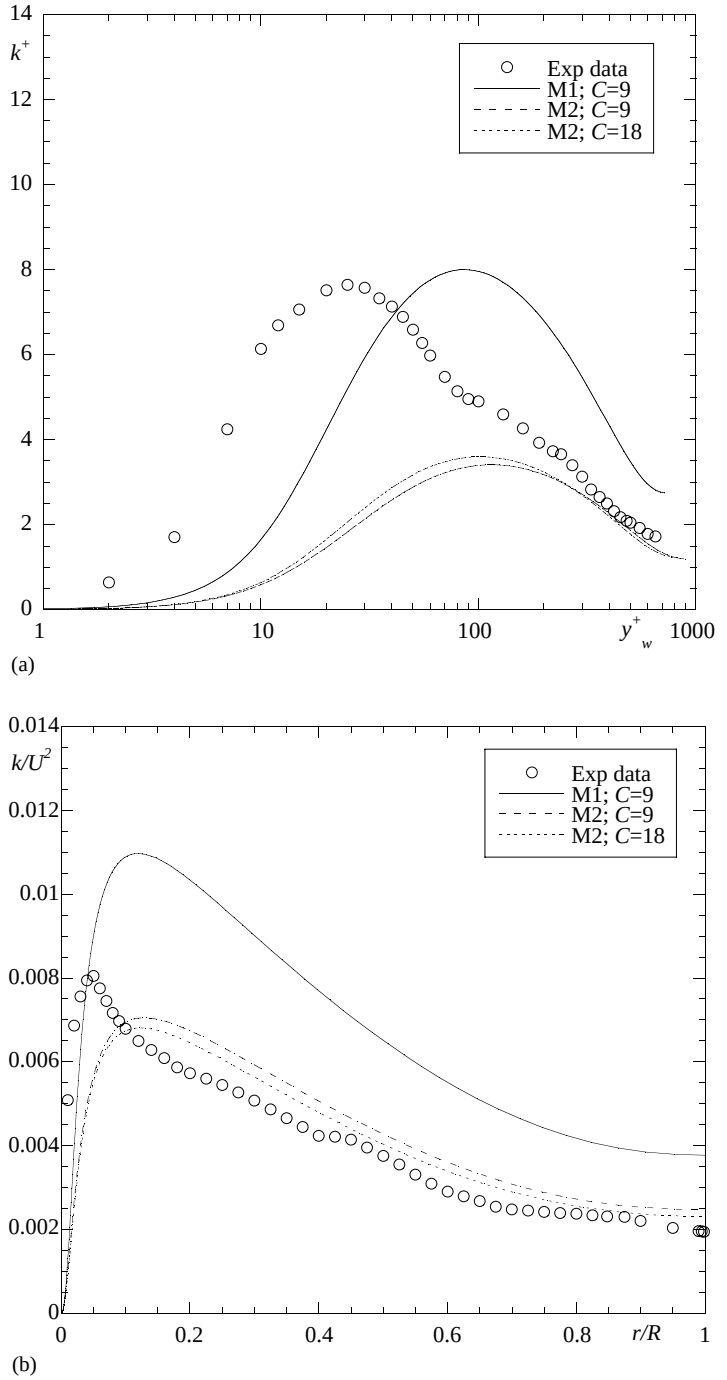

Fig. 13. Comparison between calculated ($Re_w = 39{,}000$) and experimental ($Re_w = 39{,}000$ [29]) profiles of turbulence kinetic energy for 0.2% XG solution: (a) wall normalisation; (b) physical normalisation.

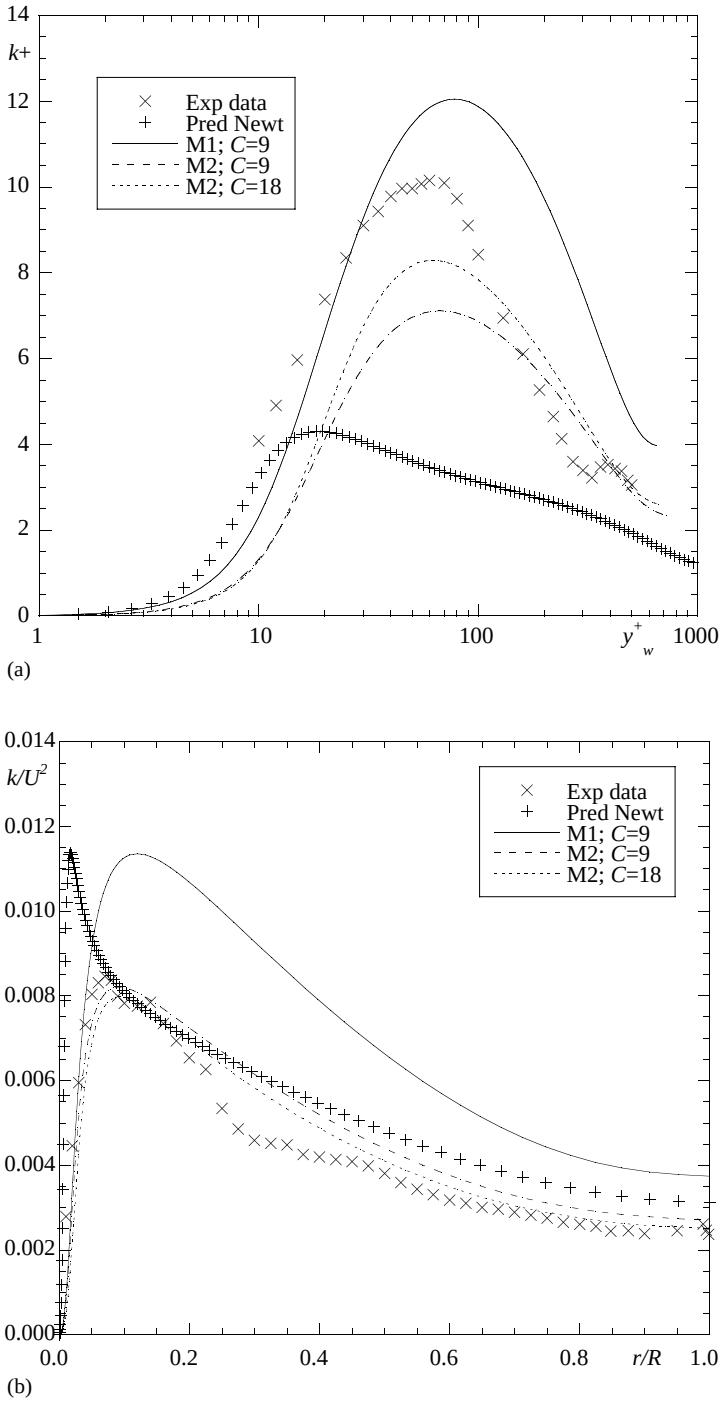

Fig. 14. Comparison between calculated ($Re_w = 42{,}400$) and experimental ($Re_w = 42{,}900$ [29]) profiles of turbulence kinetic energy for 0.125% PAA solution: (a) wall normalisation; (b) physical normalisation; for water $Re_w = 42{,}970$.

blend and less so for the PAA solution. Comparing predictions of formulation M2 with $C = 9$ and 18, the latter usually results in higher values of k^+, but the difference is small, except for the 0.125% PAA where the peak values differ by more than 15% but note this was the fluid used to optimise the values of C. However, the selection of C was based only on the values of $f - Re$ and the effect of C on the predictions of k^+ with the M2 formulation are encouraging.

Specifically, Figs. 11 and 14 compare data for the blend and the 0.125% PAA solutions with that for a Newtonian fluid at $Re_w = 42{,}970$, respectively. The Newtonian profile has the expected form with k/u_τ^2 varying from 0 at the wall, going through a maximum of 4.3 at y_w^+ around 20 and then decreasing towards the axis to a value of about 1.25 in agreement with Newtonian predictions in the literature [14]. The maximum turbulence for the non-Newtonian solutions occur always farther from the wall, with peak values for the blend with M1 larger than the Newtonian peak, but similar peak values for the 0.125% PAA and the Newtonian fluids.

For the 0.125% PAA solution the maximum value of k/U^2 of around 0.011 is just less than that of the Newtonian fluid (0.0115), and the peak is located farther from the wall, as found for drag reducing fluids by Luchik and Tiederman [36] and Gampert and Yong [37], amongst others. When the data is normalised in wall coordinates, as in Fig. 14(a), the picture is only partially consistent with the literature. The maximum value of k/u_τ^2 of 12 calculated with M1 is probably higher than it should under drag reducing conditions. Experimental works reporting data on the three components of the normal Reynolds stress are scarce, but amongst the few, Pinho and Whitelaw [38] found peak values of k/u_τ^2 in excess of

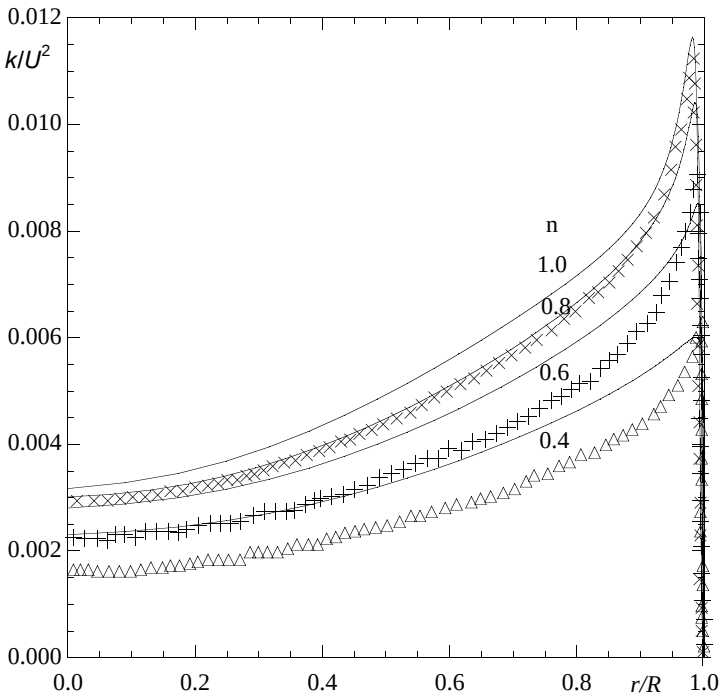

Fig. 15. Comparison between predicted and Malin's [30] profiles of turbulent kinetic energy at $Re_g = 40{,}000$ for inelastic shear-thinning fluids: (×) $n = 0.8$; (+) $n = 0.6$; (△) $n = 0.4$.

12 for aqueous solutions of CMC, and Presti's [29] data have maximum values of around 8 except for their PAA solutions where peak values higher than 12 were also measured. Clearly in excess is also the location of this peak at $y_w^+ = 70$–80 for the calculations, which is too far away from the wall, within the inertia dominated region.

The higher turbulence peak and its location farther from the wall are features also predicted before by the turbulence models quoted in Section 1 that were adapted for drag reducing flows. In the older turbulence models, peak turbulence was closer to the wall than here but, as emphasised before, those models lacked generality and were tuned for the fluids and flows to be predicted.

4.4.2. Inelastic shear-thinning fluids

For inelastic power law fluids, Fig. 15 compares predicted radial profiles of turbulent kinetic energy normalised by the bulk velocity with the numerical data of Malin [30]. For $n = 1$ our predictions agree with data from the literature for Newtonian fluids as the model becomes identical to Nagano and Hishida's low Reynolds closure [14].

As the fluid shear-thins k decreases all across the pipe. For $n = 0.8$ the prediction compares well with Malin's profile but his peak value is higher than ours. However, as n continues to decrease the reduction in k is stronger in Malin's model than in ours although the peak turbulence values tend to be identical.

Malin [30] did not plot his turbulence data in wall coordinates, hence in Fig. 16 the comparison between the various turbulent kinetic energy profiles is limited to our own results. Initially, as shear-thinning increases there is an increase in the peak value of k and the peak shifts away from the wall ($y_w^+ \approx 30$ for

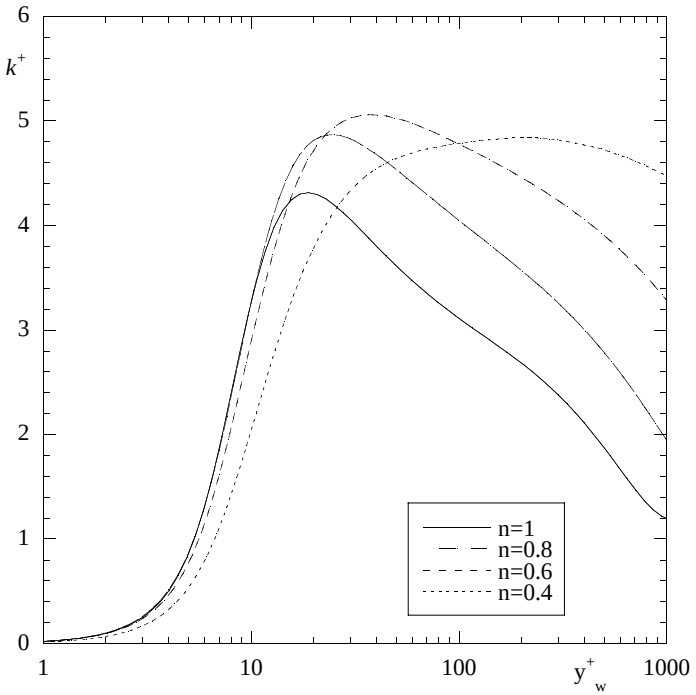

Fig. 16. Predicted variation of k with shear-thinning intensity for inelastic fluids in wall coordinates at $Re_g = 40{,}000$.

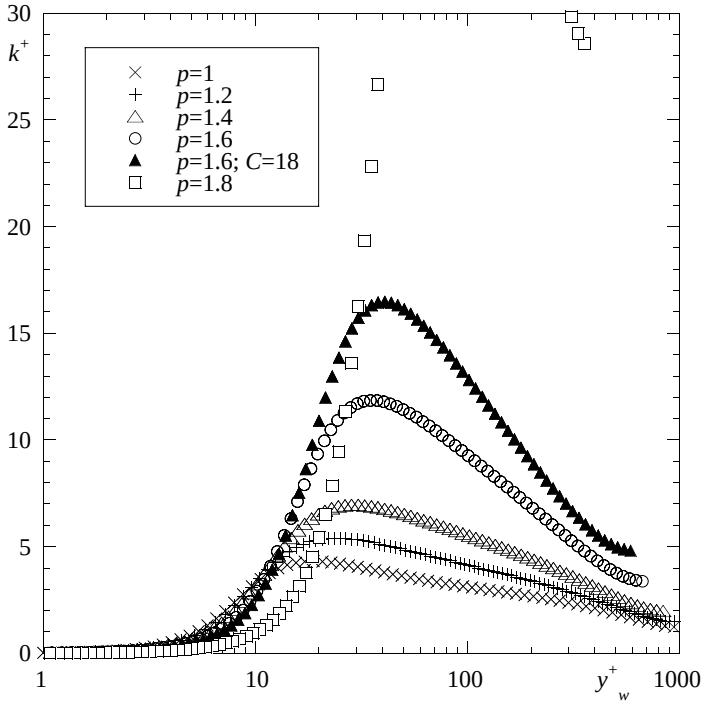

Fig. 17. Predicted variation of k for Trouton ratio thickening fluids with constant shear viscosity in wall coordinates at $Re_w = 40{,}000$ for formulation M2 with $C = 9$.

$n = 0.6$). In the viscous and buffer sublayers the profiles do not change appreciably but in the inertial sublayer and in the outer layer k^+ increases substantially. When n further decreases new changes arise: the viscous sublayer thickens, the peak value of k^+ slightly decreases but now it occurs over a broader region; the peak value of k^+ now occurs at about 200 wall units. This is caused by the extreme shear-thinning intensity and the very low value of the wall viscosity. Figs. 15 and 16 correspond to a constant generalised Reynolds number but the wall Reynolds number varies from 40,000 for $n = 1$ to 850,000 for $n = 0.4$.

4.4.3. Trouton ratio thickening fluids

The effect of strain-hardening of the extensional viscosity on $k^+ - y^+_w$ for fluids with constant shear-viscosity can be seen in Fig. 17. It is obvious again an increase in the peak value of k^+ with p as DR is intensified. For $p = 1.8$ it was previously seen that Virk's maximum DR asymptote for f and Virk's ultimate velocity profile for u^+ had been exceeded and the corresponding profile of k^+ has overshoot with a peak value of the order of 70, about 7 times the peak value of k^+ for $p = 1.6$ and $C = 9$. Increasing C from 9 to 18 for $p = 1.6$ increases k^+ significantly because of its better capacity to predict DR (see Fig. 4). Note also that the peak k^+ of 16 for $C = 18$ is in excess of values seen in the literature on experiments for drag reducing fluids.

It is also interesting to notice that as the peak increases it takes place farther away from the wall, as was seen in the previous section for the effect of n. However, whereas the peak value of k^+ changed little with n it varies significantly with p. This is in agreement with the contrasting effects of n and p on f: whereas n had a small effect, the value of p is crucial to determine the amount of DR. In terms of the location of

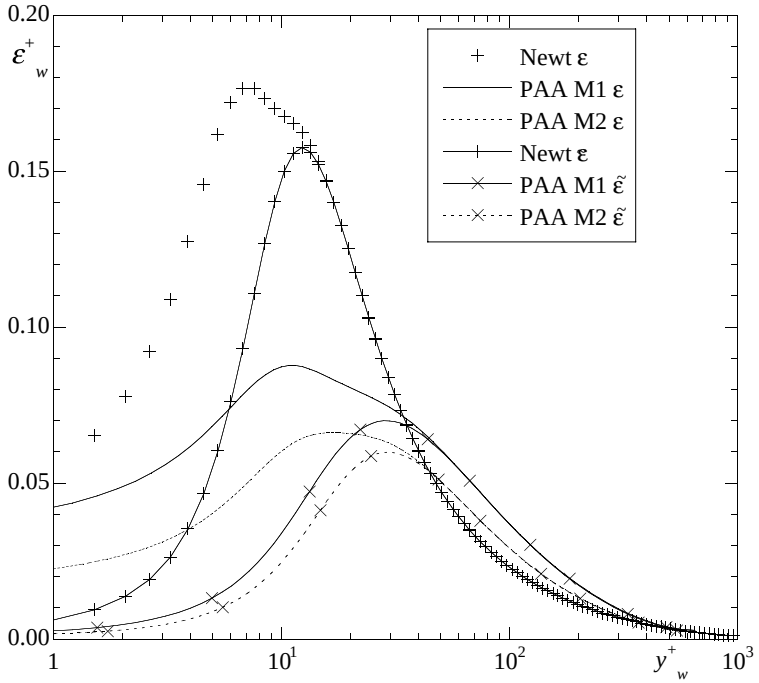

Fig. 18. Radial variation of the normalised rate of dissipation of turbulence kinetic energy in pipe flow in wall coordinates. Comparison between predictions of Newtonian and 0.125% PAA flows with formulations M1 and M2 at $Re_w = 42{,}900$ with $C = 9$.

the peak value of k^+ both n and p have similar influences: the peak value of k^+ of 11.9 for $p = 1.6$ occurs at 35 wall units, whereas for $p = 1$ it is located at $y^+_w \approx 15$; a similar quantitative variation takes place when n goes from 1 to 0.6. As a consequence, the large deviation seen previously for the peak value of 0.125% PAA is the result of the combined effects of n and p whereas the intense DR is mostly due to p.

4.5. Other quantities

No other experimental data are available in [9], so the following comparisons are between predictions for a Newtonian fluid and a specific polymer solution. The choice is again the 0.125% PAA solution used in Section 4.1.1 to determine parameter C and the comparisons are made at the same wall Reynolds number of 42,900, which corresponds to the set of experimental data for 0.125% PAA in [9]. Of interest are comparisons of the radial profiles of the rate dissipation of turbulence kinetic theory, the shape of the damping functions and the various viscosities in an attempt to shed light onto the characteristics of the new turbulence model and its shortcomings, to guide future developments and improvements. Only predictions obtained for $C = 9$ are presented here to avoid cluttered figures. Anyway, for M2 with $C = 18$ the profiles are intermediate to those for M1 and M2 with $C = 9$.

Using wall normalisation ($\varepsilon^+ = \varepsilon \nu_w / u_\tau^4$), Fig. 18 shows the radial variation of ε and $\tilde{\varepsilon}$. Whereas the modified dissipation $\tilde{\varepsilon}$ tends to zero at the wall, the true dissipation does not, but outside the viscous and buffer layers the two quantities are identical.

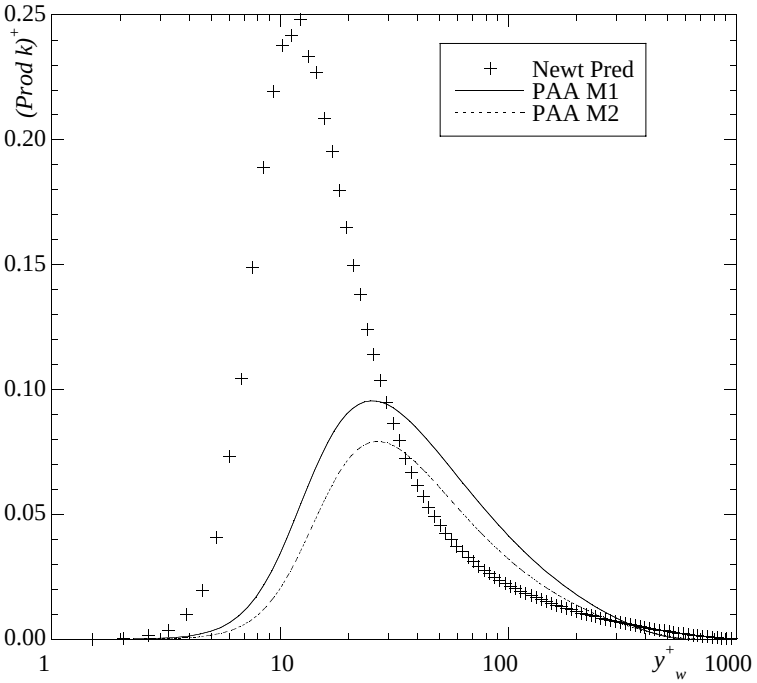

Fig. 19. Radial variation of the normalised production of k in pipe flow in wall coordinates. Comparison between predictions of Newtonian and 0.125% PAA flows with formulations M1 and M2 at $Re_w = 42{,}900$ with $C = 9$.

The curves for PAA and the Newtonian fluid are not too different in shape but differ in magnitude. The peak value of ε^+ occurs at $y_w^+ = 7$ for the Newtonian fluid and at $y_w^+ = 10$ for the PAA, but the latter is only half the value for water. So, whereas for the Newtonian fluid, the peak dissipation occurs close to the peak turbulence kinetic energy, for the PAA fluid the peak dissipation happens closer to the wall than the peak k. In terms of ε the differences between Newtonian and PAA predictions are less than in terms of k. Lower rates of dissipation for drag reducing fluids, agree with findings from various authors who performed DNS simulations with FENE-P fluids: Dimitropoulos et al. [39] and De Angelis et al. [40]. These numerical works, and the measurements of Den Toonder et al. [41], Warholic et al. [7] and Ptasinski et al. [16] also reported a Reynolds stress deficit due to the appearance of an extra stress associated with the polymer additive. The reduction in Reynolds shear stress leads to a decrease in turbulence production, a feature again predicted in the current simulations, as can be seen in Fig. 19.

The ordinate in Fig. 19 is the production of turbulent kinetic energy normalised with wall coordinates, i.e.,

$$(\text{Prod}\, k)^+ = -\overline{uv}^+ \frac{\partial U^+}{\partial y^+}. \tag{58}$$

The peak production for drag reducing solutions is 40% of that for the water flows and whereas the peak production is at $y_w^+ \approx 12$ for a Newtonian fluid it moves to $y_w^+ \approx 22$ for the PAA solution confirming a wider buffer layer typical of drag reducing flows.

The corresponding radial profiles of shear stress are compared in Fig. 20. For the Newtonian fluid the shear stress varies linearly in the 80% central region of the pipe in accordance to a momentum balance

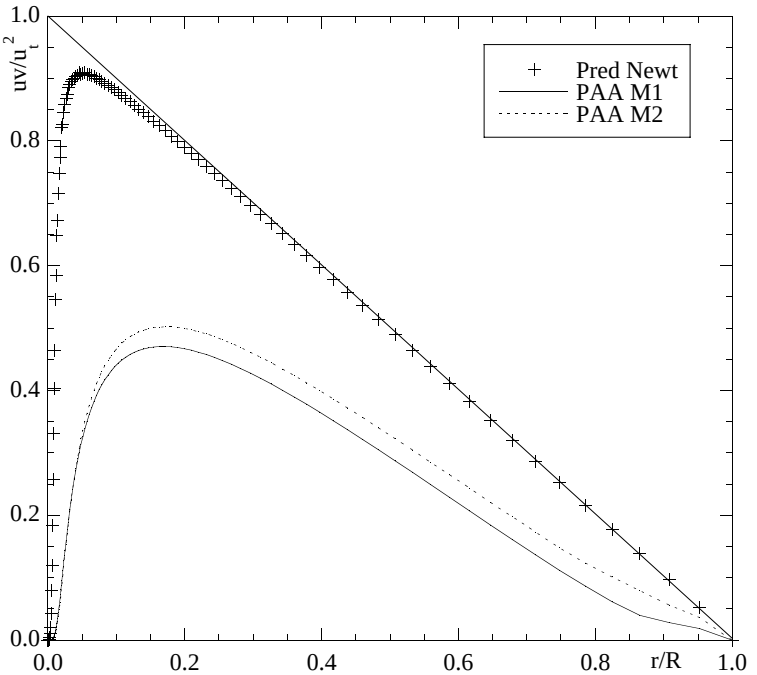

Fig. 20. Radial variation of the normalised Reynolds shear stress in pipe flow. Comparison between predictions of Newtonian and 0.125% PAA flows with formulations M1 and M2 at $Re_w = 42{,}900$ with $C = 9$.

with negligible molecular shear stress. However, the 0.125% PAA solution shows a Reynolds shear stress deficit, with formulation M1 predicting the highest deficit in agreement with its higher DR. As far as the peak turbulent shear stress is concerned its location is farther from the wall for the polymer solution, regardless of the damping function adopted and its numerical value is half that for Newtonian fluids. The reasons for this behaviour will become clear below in the analysis of the radial variations of the damping function f_μ and of the various viscosities.

The Newtonian, M1 and M2 damping functions f_μ are compared in Fig. 21. Whereas the Newtonian damping function varies from zero at the wall to 1 at about $y_w^+ = 300$, the viscoelastic f_μ for M1 barely exceeds 0.025 and slightly drops on approaching the axis of the pipe. The M2 function f_μ is less damping, reaching 0.14 on axis. Since f_μ is also used for the molecular viscosity (cf. $f_\nu = f_\mu$ in Eq. (8)), the weighted molecular viscosity $\bar{\mu}$ remains basically unaffected by turbulence ($\bar{\mu}_h$) and is given by the laminar expression (Eq. (3)) except in the central region of the pipe because whenever $\bar{\mu}$ exceeded $\bar{\mu}_h$ we set $\bar{\mu} = \bar{\mu}_h$. The small drop of the M1 f_μ at the pipe centre is a consequence of the very high local viscosity given by the power law,[4] which was fitted to the intense shear-thinning viscosity behaviour of the 0.125% PAA, since in this formulation it is the local viscosity that is used to define y^+ (cf. Eq. (21)). By using a constant viscosity to define y_w^+ this feature is removed as can be seen in the profile of f_μ for M2.

[4] On axis the viscosity should be infinite but a constant viscosity was imposed for shear rates below $10^{-3}\,s^{-1}$ to remove the singularity. A second limiter, defined on physical grounds in the core of the pipe, was set to $\bar{\mu}$ instead of η_v and was $\bar{\mu}_{max} = \bar{\mu}_h$. Note that many real fluids have constant zero shear viscosities and consequently this problem does not occur.

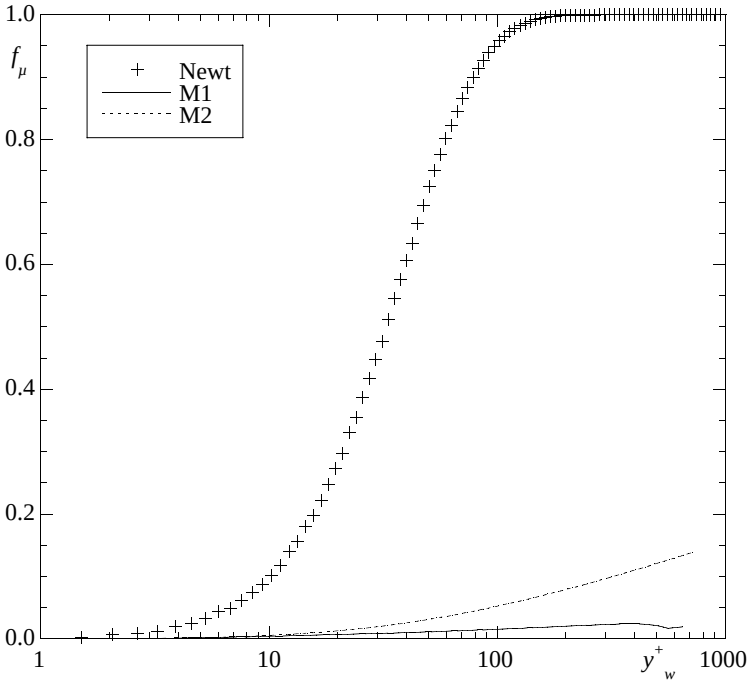

Fig. 21. Variation of the damping function f_μ in wall coordinates. Results with formulations M1 and M2 for 0.125% PAA solution using $C = 9$.

At this stage it is interesting to compare the transverse variations of the various viscosities in Fig. 22. The shear viscosity η_v follows a power law and consequently tends to infinity at the centre line, an undesirable feature removed by using viscosity limiters ($\bar{\mu} = \bar{\mu}_h$ whenever $\bar{\mu}$ exceeded $\bar{\mu}_h$). Over most of the pipe $\bar{\mu}_h$ is larger than the pure shear viscosity η_v due to the effect of turbulence, as would be expected on the grounds of the theory outlined in the first part of this work [10]. However, the large damping introduced by $f_v = f_\mu$ makes $\bar{\mu}$ (given by Eq. (8)) basically identical to η_v. Simultaneously, the turbulent viscosity is also strongly reduced by f_μ, taking values of the order of magnitude of the molecular viscosity. This is clear in Fig. 20 where the Reynolds shear stress is not much different from the molecular shear stress over the whole pipe.

Reynolds stress deficits have been reported in both experimental [7,8,16,42] and direct numerical simulations [39] of drag reducing flows. The measured values of the Reynolds shear stress in the log-law region are usually well above those of the molecular shear stress and in some instances the sum of both can account for about 2/3 of the total stress produced by the pressure gradient. The remaining 1/3 of the total stress, the Reynolds stress deficit, is due to an extra stress of viscoelastic origin accounting for interactions between molecular and turbulent events. In the momentum equations used here such stress is represented by both $2\bar{\mu}S_{ij}$ and $2\overline{\mu' s_{ij}}$ seen to be important in [10]. The latter term was neglected in this work but it still needs to be modelled to improve prediction quality.

Since the predictions of this turbulence model were adjusted to experimental data by selecting the value of C, the momentum balance is respected with the role of $2\overline{\mu' s_{ij}}$ taken by the purely viscous term $2\bar{\mu}S_{ij}$ and the strong dampening of $\bar{\mu}$ brought by f_v but this substitution is not equivalent. The excessive role played

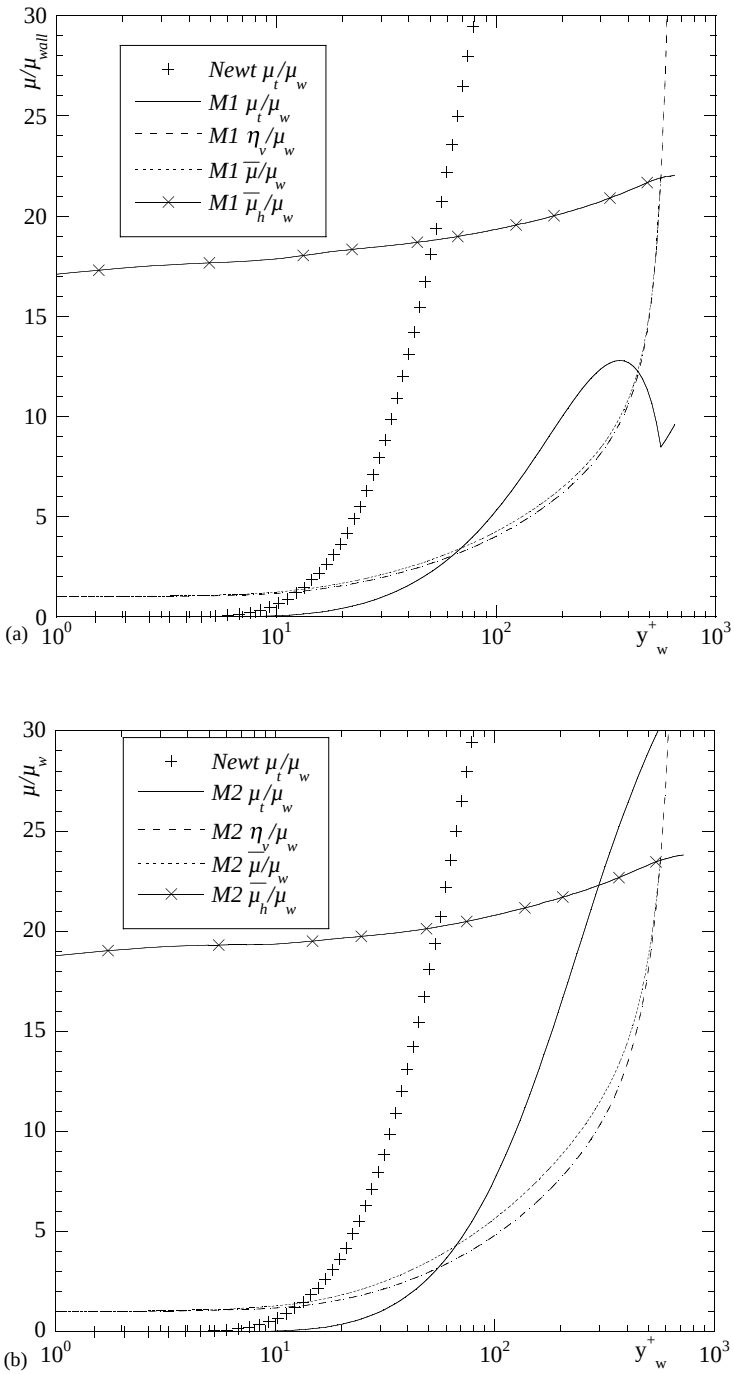

Fig. 22. Variation of the normalised viscosities for the 0.125% PAA and Newtonian flows at $Re_w = 42{,}900$ and $C = 9$: (a) M1; (b) M2.

by damping functions f_ν and f_μ are undesirable features which were possible here because of the adoption of a rheological equation accounting for the combined effects of shear-thinning, strain-thickening and turbulence on the viscosity, which in addition allowed the derivation of the damping functions to be done systematically. However, these two strategies are not equivalent in terms of the turbulence model: proper account of $2\overline{\mu' s_{ij}}$ should reduce the impact of f_μ and f_ν while maintaining the same DR capability, and possibly affecting favourably the balance between the turbulent quantities $\overline{uv}$, k and ε.This will not release us from the use of damping functions, as is known from Newtonian modelling, but under such conditions the numerical value of C could then be reduced from the present values of 9 or 18.

This constitutes the next major improvement of the present turbulence model. Still, this closure constitutes a breakthrough in the current framework because it is the first model able to predict turbulent drag reducing flows of viscoelastic fluids, including the purely viscous case, which only uses as input rheological parameters of the fluid.

This turbulence closure is able to predict strong DR, higher than for purely shear-thinning fluids and it predicts a positive shift in the inertial sublayer as well as an increase in its slope, deviations of the peaks in k and ε to locations farther away from the wall, reductions in the peak values of k and ε, reductions in production of k and the Reynolds shear stress deficit. All these features have been observed experimentally in the past and are associated with a Trouton ratio thickening behaviour that researchers around the world have related to the drag reducing phenomenon, although that has not been demonstrated beyond doubt. It is true that these features were obtained with a model derived from a too simplistic rheological constitutive equation, but this was a way to arrive at a closed form of all equations and constitutes a major step forward towards more realistic Reynolds averaged turbulence closures.

By its nature, the k–ε closure assumes isotropic turbulence and it is well known that in turbulent pipe flows this is not the case and especially so with viscoelastic drag reducing fluids. The Reynolds stress anisotropy enhancement associated with DR is one of the important features that we expect to capture in the near future in the current development of a Reynolds stress closure based on this work and that of Pinho [10].

5. Conclusions

A low Reynolds number version of the k–ε model derived in [10] was finalised and used to predict turbulent pipe flow of various polymer solutions. The model was built on top of the Newtonian model of Nagano and Hishida and it reduces to it in the limit of constant viscometric and extensional viscosities. To complete the model, a new viscous damping function f_μ had to be derived to account for both viscometric and extensional viscosity effects. A second damping function f_ν was introduced and made equal to f_μ after a parametric investigation. The extra term in the dissipation equation was found to have a positive role on turbulent quantities although it had a small effect upon the mean velocity profile and friction factor.

The current turbulence model can predict fairly well the friction factor behaviour of polymer solutions under drag reducing conditions and a new model parameter C was also quantified ($C = 9$ or 18, the latter value being our recommendation to be used with formulation M2 of the damping function).

Under drag reducing conditions, the turbulence model was able to predict satisfactorily mean velocity profiles, the reductions in k, ε and in the production of k, the shift of their peaks away from the wall and the appearance of a Reynolds shear stress deficit. The damping function recommended is M2 and uses the wall viscosity to compute the wall coordinate y_w^+. For inelastic shear-thinning fluids, predictions by

model M2 also agree well with the correlations available in the literature for friction factor and mean velocity.

The functions f_μ and f_v were seen to be too damping probably due to the lack of a model for term $2\overline{\mu' s_{ij}}$ in the momentum equation and solution of this shortcoming constitutes the next required improvement of the present turbulence closure. This work constitutes a first step towards developing better single-point turbulence closures for viscoelastic turbulent flows and further investigations must be pursued along two different paths:

(1) Improvements to the current turbulence model (as mentioned) including the development of more advanced models to predict the full Reynolds stress tensor, but based on the same or closely related rheological constitutive equation of the generalised Newtonian type.
(2) The adoption of more advanced and realistic viscoelastic constitutive equations that are able to predict shear-thinning, Trouton ratio thickening and the existence of normal stresses, such as the FENE-P model. With such rheological equation, a totally new turbulence model should then be developed following procedures akin to those exposed here and in the previous work [10].

Acknowledgements

The authors wish to thank CNPq of Brasil and ICCTI of Portugal for funding the exchange programme Project 2001 Proc C 4.3.1. F.T. Pinho also acknowledges the financial support of FEDER awarded by Fundação para a Ciência e Tecnologia through grants POCTI 37699/EQU/2001 and POCTI 37711/EME/2001. We are also in debt to Profs. P.J. Oliveira (Universidade da Beira Interior, Portugal), B.A. Younis (former City University, UK, now at University of California, US), C.E. Maneschy (Universidade Federal do Pará, Brasil) and M.P. Escudier (University of Liverpool, UK) for many valuable discussions. We are also thankful to Prof. M.P. Escudier for making available the turbulent data of Presti [29].

References

[1] T. Mizushina, H. Usui, T. Yoshida, Turbulent pipe flow of dilute polymer solutions, J. Chem. Eng. Jpn. 7 (3) (1973) 162–167.
[2] S. Hassid, M. Poreh, A turbulent energy model for flows with drag reduction, Trans. ASME J. Fluids Eng. 97 (1975) 234–241.
[3] S. Hassid, M. Poreh, A turbulent energy dissipation model for flows with drag reduction, J. Fluids Eng. 100 (March) (1978) 107–112.
[4] M. Poreh, S. Hassid, Mean velocity and turbulent energy closures for flows with drag reduction, Phys. Fluids 20 (10) (1977) S193–S196.
[5] F. Durst, A.K. Rastogi, Calculations of turbulent boundary layer flows with drag reducing polymer additives, Phys. Fluids 20 (12) (1977) 1975–1985.
[6] S. Politis, Turbulence modelling on inelastic power law fluids, Internal Report, Department of Mechanical Engineering, Imperial College, UK, also Internal Report of Brite Project RIIB.0085.UK (H), 1989.
[7] M.D. Warholic, H. Massah, T.J. Hanratty, Influence of drag reducing polymers on turbulence: effects of Reynolds number, concentration and mixing, Exp. Fluids 27 (1999) 461–472.
[8] M.D. Warholic, D.K. Heist, M. Katcher, T.J. Hanratty, A study with particle-image velocimetry of the influence of drag-reducing polymers on the structure of turbulence, Exp. Fluids 31 (2001) 474–483.
[9] M.P. Escudier, F. Presti, S. Smith, Drag reduction in the turbulent pipe flow of polymers, J. Non-Newtonian Fluid Mech. 81 (1999) 197–213.
[10] F.T. Pinho, A GNF framework for turbulent flow models of drag reducing fluids and proposal for a k–ε type closure, J. Non-Newtonian Fluid Mech. 114 (2–3) (2003) 149–184.

[11] H.A. Barnes, J.F. Hutton, K. Walters, An Introduction to Rheology, Elsevier, Amsterdam, 1989.
[12] V.C. Patel, W. Rodi, G. Scheuerer, Turbulence models for near-wall and low-Reynolds number flows: a review, AIAA J. 23 (9) (1985) 1308–1319.
[13] S.B. Pope, Turbulent Flows, Cambridge University Press, Cambridge, UK, 2000.
[14] Y. Nagano, M. Hishida, Improved form of the k–ε model for wall turbulent shear flows, J. Fluids Eng. 109 (1987) 156.
[15] A.S. Pereira, F.T. Pinho, Turbulent pipe flow characteristics of low molecular weight polymer solutions, J. Non-Newtonian Fluid Mech. 55 (1994) 321–344.
[16] P.K. Ptasinski, F.T.M. Nieuwstadt, B.H.A.A. Van den Brule, M.A. Hulsen, Experiments in turbulent pipe flow with polymer additives at maximum drag reduction, Flow Turbulence Combust. 66 (2001) 159–182.
[17] B.J.S. Barnard, R.H.J. Sellin, Grid turbulence in dilute polymer solutions, Nature 222 (June) (1969) 1160–1162.
[18] C.A. Greated, Effect of polymer additive on grid turbulence, Nature 224 (December) (1969) 1196–1197.
[19] W.D. McComb, J. Allan, C.A. Greated, Effect of polymer additives on the small-scale structure of grid-generated turbulence, Phys. Fluids 20 (6) (1977) 873–879.
[20] C.A. Friehe, W.H. Schwarz, Grid-generated turbulence in dilute polymer solutions, J. Fluid Mech. 44 (1970) 173–193.
[21] E.R. Van Driest, On turbulent flow near a wall, J. Aeronaut. Sci. 23 (1956) 1007–1011.
[22] D.O.A. Cruz, C.E. Maneschy, E.N. Macêdo, J.N.N. Quaresma, A turbulence model for computing the flow of power law fluids within circular tubes, Hybrid Meth. Eng. 2 (2000) 1–13.
[23] D.W. Dodge, A.B. Metzner, Turbulent flow of non-Newtonian systems, AIChE J. 5 (2) (1959) 189–204.
[24] N.E. Hudson, T.E.R. Jones, The A1 project—an overview, J. Non-Newtonian Fluid Mech. 46 (1993) 69–88.
[25] J.S. Schulze, T.P. Lodge, C.W. Macosko, J. Hepperle, H. Münstedt, H. Bastian, D. Ferri, D.J. Groves, Y.H. Kim, M. Lyon, T. Schweizer, T. Virkler, E. Wassner, W. Zoetelief, A comparison of extensional viscosity measurements from various RME rheometers, Rheol. Acta 40 (2001) 457–466.
[26] C.G. Hermansky, D.V. Boger, Opposing jet viscometry of fluids with viscosity approaching that of water, J. Non-Newtonian Fluid Mech. 56 (1995) 1–14.
[27] G.G. Fuller, C.A. Cathey, B. Hubbard, B.E. Zebrowski, Extensional viscosity measurements for low-viscosity fluids, J. Rheol. 31 (3) (1987) 235–249.
[28] P. Dontula, M. Pasquali, L.E. Scriven, C.W. Macosko, Can extensional viscosity be measured with opposed nozzle devices? Rheol. Acta 36 (1997) 429–448.
[29] F. Presti, Investigation of transitional and turbulent pipe flow of non-Newtonian fluids, Ph.D. Thesis, University of Liverpool, UK, 2000.
[30] M.R. Malin, Turbulent pipe flow of power-law fluids, Int. Commun. Heat Mass Transfer 24 (7) (1997) 977–988.
[31] B.A. Younis, A computer program for two-dimensional turbulent boundary-layer flows, Internal Report, Department of Civil Engineering, City University, London, UK, 1987.
[32] P.S. Virk, H.S. Mickley, K.A. Smith, The ultimate asymptote and mean flow structure in Tom's phenomenon, J. Appl. Mech. 92 (June) (1970) 488–493.
[33] C.K.G. Lam, K. Bremhorst, A modified form of the k–ε model for predicting wall turbulence, J. Fluids Eng. 103 (1981) 456–460.
[34] P.S. Virk, Drag reduction fundamentals, AIChE J. 21 (4) (1975) 625–656.
[35] A.H.P. Skelland, Non-Newtonian Flow and Heat Transfer, Wiley, New York, 1967.
[36] T.S. Luchik, W.G. Tiederman, Turbulent structure in low concentration drag reducing channel flows, J. Fluid Mech. 190 (1988) 241–263.
[37] B. Gampert, C.K. Yong, The influence of polymer additives on the coherent structure of turbulent channel flow, in: A. Gyr (Ed.), Structure of Turbulence and Drag Reduction, IUTAM Symposium, Zürich, 1989, Springer, Berlin, 1990, pp. 223–232.
[38] F.T. Pinho, J.H. Whitelaw, Flow of non-Newtonian fluids in a pipe, J. Non-Newtonian Fluid Mech. 34 (1990) 129–144.
[39] C.D. Dimitropoulos, R. Sureshkumar, A.N. Beris, R.A. Handler, Budgets of Reynolds stress, kinetic energy and streamwise enstrophy in viscoelastic turbulent channel flow, Phys. Fluids 13 (4) (2001) 1016–1027.
[40] E. De Angelis, C.M. Casciola, R. Piva, DNS of wall turbulence: dilute polymers and self-sustaining mechanisms, Comput. Fluids 31 (2002) 495–507.
[41] J.M.J. Den Toonder, M.A. Hulsen, G.D.C. Kuiken, F.T.M. Nieuwstadt, Drag reduction by polymer additives in a turbulent pipe flow: numerical and laboratory experiments, J. Fluid Mech. 337 (1997) 193–231.
[42] W.W. Willmarth, T. Wei, C.O. Lee, Laser anemometer measurements of Reynolds stress in a turbulent channel flow with drag reducing polymer additives, Phys. Fluids 30 (4) (1987) 933–935.